

Article

An Efficient Computer Vision-Based Dual-Face Target Precision Variable Spraying Robotic System for Foliar Fertilisers

Chengtian Zhu ¹, Shuaihua Hao ¹, Cailing Liu ^{1,*}, Yuewei Wang ¹, Xuan Jia ¹, Jitong Xu ¹, Songbao Guo ¹, Juxin Huo ¹ and Weiming Wang ²

¹ College of Engineering, China Agricultural University, Beijing 100083, China; chengtianzhu1029@cau.edu.cn (C.Z.); s20233071562@cau.edu.cn (S.H.); wyw2022.a@gmail.com (Y.W.); b20213070591@cau.edu.cn (X.J.); xujitong0718@cau.edu.cn (J.X.); s20243071655@cau.edu.cn (S.G.); sy20243071674@cau.edu.cn (J.H.)

² School of Agricultural Engineering, Jiangsu University, Zhenjiang 212013, China; 3210306020@stmail.ujs.edu.cn

* Correspondence: cailingliu@cau.edu.cn

Abstract: The application of foliar fertiliser can rapidly replenish the essential nutrients required by crops. In order to enhance the precision of foliar fertiliser spraying, fertiliser utilisation, and leaf absorption efficiency, this study proposes the implementation of an efficient foliar fertiliser dual-face target precision variable spraying robot system based on computer vision. In this study, we propose the SN-YOLOX Nano-ECA as a real-time classification model for potted plants. The model has parameters and FLOPs of only 0.48 M and 0.16 G, respectively. Following deployment, the classification precision and recall reached 97.86% and 98.52%, respectively, with an FPS of 37.6. A dual-face target precision variable spraying method of foliar fertiliser based on the determination of leaf area and plant height information of potted plants was proposed. A robot platform for the application of foliar fertilisers was developed, and a positioning and navigation system based on the RSSI principle was constructed. The results of the foliar fertiliser spraying experiments demonstrate that the precision of the extracted leaf area and height information is above 97% and 96%, respectively. The navigation system demonstrated distance and angle errors of only 5.598 cm and 0.2245°. The mean discrepancy between the actual and set spraying volumes was 0.46 mL. This robotic system is capable of precise spraying of foliar fertiliser, which provides a new idea and reference for the development of efficient and precise variable spraying technology for foliar fertiliser.

Keywords: foliar fertiliser; potted plants; SN-YOLOX Nano-ECA model; spraying method; robot platform



Citation: Zhu, C.; Hao, S.; Liu, C.; Wang, Y.; Jia, X.; Xu, J.; Guo, S.; Huo, J.; Wang, W. An Efficient Computer Vision-Based Dual-Face Target Precision Variable Spraying Robotic System for Foliar Fertilisers. *Agronomy* **2024**, *14*, 2770. <https://doi.org/10.3390/agronomy14122770>

Received: 21 October 2024

Revised: 13 November 2024

Accepted: 18 November 2024

Published: 22 November 2024



Copyright: © 2024 by the authors. Licensee MDPI, Basel, Switzerland. This article is an open access article distributed under the terms and conditions of the Creative Commons Attribution (CC BY) license (<https://creativecommons.org/licenses/by/4.0/>).

1. Introduction

The application of fertilisers is of vital importance in the context of increasing crop yields and safeguarding plant growth [1–3]. Indeed, fertilisers represent an indispensable component of modern agricultural practice. The judicious use of fertilisers can regulate crop growth and also improve crop yields and quality [4,5]. Conventional fertilisation operations primarily supply the nutrients essential for crop growth through soil and irrigation application [6]. However, these methods encounter challenges such as suboptimal nutrient utilisation and the risk of environmental pollution [7]. In response to these limitations, precision variable fertiliser application has emerged as a promising avenue in modern agricultural research [8]. This approach can substantially enhance the precision of fertilisation operations while mitigating environmental stress [9,10].

Precision variable fertilisation is an efficient fertilisation technology [11] which enables dynamic adjustments to the fertilisation strategy based on real-time crop growth monitoring, significantly enhancing the efficiency of fertiliser utilisation [12]. Based on the optimal matching strategy, Zhang et al. proposed a method of reducing the basal fertiliser and increasing the follow-up fertiliser (RBIT) use with the return of rice straw to the field,

allowing for the precise variable fertilisation of rice and thereby improving yield stability [13]. Zhu et al. designed an electronically controlled precise variable fertilisation system based on the method of PID controller and a particle swarm optimisation algorithm [14,15], which solved the problem of insufficient control accuracy in the traditional air-assisted side-depth fertilisation equipment for the variable fertilisation of rice.

Foliar fertiliser spraying technology allows for the rapid replenishment of essential nutrients required for crop growth by applying fertiliser directly to the surface of plant leaves [16]. Currently, foliar fertiliser sprays are predominantly deployed using agricultural drones and sprayers [17], which atomise liquid fertiliser into fine particles and spray them on the surface of plant leaves, increasing the contact area with the leaves and improving the efficiency of nutrient absorption [18]. The precise spraying of foliar fertiliser can be achieved through the fusion of multiple sensors and computer vision [19], thus improving fertiliser utilisation and reducing environmental pollution. Zong et al. devised a real-time positioning system and fertiliser application control system for maize seedling cores based on computer vision [20], which enabled the implementation of intelligent and efficient fertiliser management through the minimum cross-entropy image segmentation method. Gao et al. developed an intelligent system that combines computer vision, machine learning, and a cuckoo search algorithm dedicated to accurate fertiliser application decision-making for maize, rice, and soybeans [21], which facilitated the management of large areas of farmland. These systems are primarily designed for field crops, which require high-precision sensors and intricate image processing systems and have poor adaptability to environmental conditions. The application of foliar fertiliser spraying technology based on computer vision has more advantages in the relatively stable environments of crop facilities. However, there is no relevant application in this field. The root development of potted plants cultivated in facilities is frequently impeded by spatial limitations, which renders the uptake of nutrients particularly challenging. The implementation of rational foliar area fertilisation practices can prevent and rectify physiological disorders, such as yellowing caused by deficiencies, thereby enabling optimal growth status.

In light of the above, this study proposes the implementation of a computer vision-based foliar fertiliser dual-face target precision variable spraying robotic system, which integrates target identification and classification, a foliar fertiliser spraying method, and a spraying operation robotic platform. As illustrated in Figure 1, the system is capable of autonomous localisation, navigation, and movement during the foliar fertiliser spraying operation. It also collects real-time plant images after the local camera detects the potted plant target. The system makes foliar fertiliser spraying decisions according to the obtained plant class, height, and leaf area information, and the controller's output signals control the end-actuator action to complete the foliar fertiliser spraying operation. The controller generates signals that control the end-effector action, thereby achieving dual-face target precision variable foliar fertiliser spraying. During the spraying operation, the end-actuator determines the required amount of foliar fertiliser based on the decision-making result and then adjusts the height and angle of the upper and lower spray nozzles on both sides through the slide and 2D gimbal. The fertiliser pipe then outputs this determined amount, completing the spraying operation.

The principal specific contributions of this study are as follows: Firstly, a lightweight real-time target classification model, designated SN-YOLOX Nano-ECA, was developed for potted plants. Additionally, a dual-face target precision spraying method for foliar fertilisers was proposed. Furthermore, a self-propelled robotic operating platform, which efficiently and precisely targets spraying of foliar fertilisers, was constructed. In this study, dual-face target precision variable spraying of foliar fertiliser was achieved according to the class and phenotypic information of potted plants. This study aims to reduce the use of foliar fertiliser and improve the utilisation rate of foliar fertiliser, thereby promoting the development of agriculture in a more environmentally friendly, efficient, and sustainable direction.

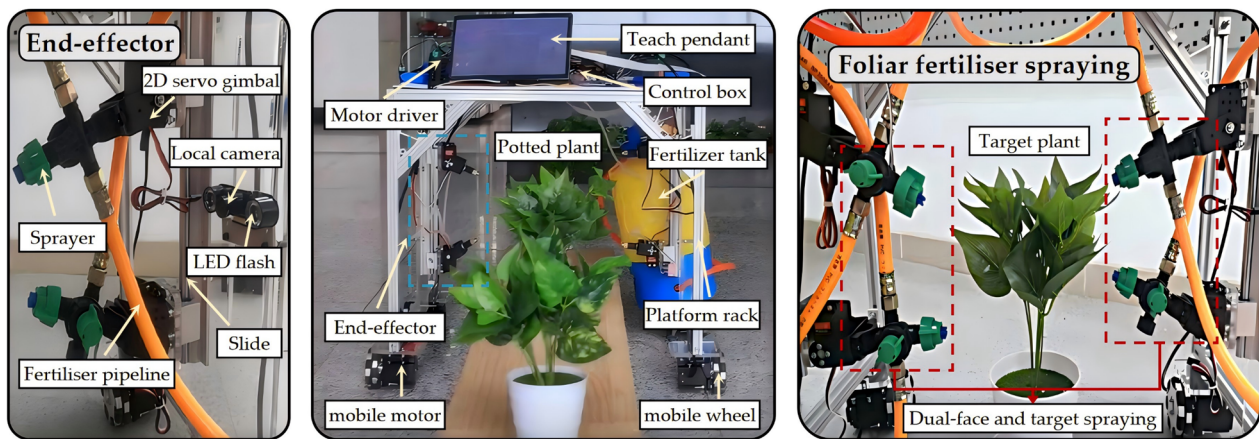


Figure 1. Proposed dual-face target precision variable spraying robot system.

2. Materials and Methods

2.1. Identification and Classification of Potted Plants

2.1.1. Image Acquisition and Dataset Construction

To ensure the model fully learns image features, it is essential to select images with appropriate brightness, resolution, and contrast as the dataset for training. In this study, an image dataset was assembled and labelled, comprising specimens of *Rohdea japonica*, *Aglaonema modestum*, *Dieffenbachia seguine*, and *Codiaeum variegatum*. These four potted plants are popular indoor ornamental potted plants in China and exhibit distinctive specific leaf patterns despite their nearly oval shapes. The leaf colours of *Rohdea japonica*, *Aglaonema modestum*, and *Dieffenbachia seguine* are predominantly dark green, while *Codiaeum variegatum* is characterised by a combination of yellow and dark green. *Rohdea japonica* and *Aglaonema modestum* have no discernible patterning on their leaves, *Dieffenbachia seguine* has irregular white markings, and *Codiaeum variegatum* features yellow-orange stripes and spots. The image data were acquired from January to March 2024 within the Laboratory of Modern Design and Advanced Manufacturing of Agricultural Equipment (116.357754 E, 40.006264 N) at China Agricultural University, Beijing, China. Images gathered in real time in a genuine identification environment may encompass a range of viewpoints and lighting conditions. To ensure the diversity of the samples, the richness of the image dataset, and the robustness of the training model, images of potted plants were collected at different times of the day from different shooting angles with different occlusion conditions using a Canon EOS R7 camera (Canon, Tokyo, Japan) with a resolution of 4800×4800 and a shooting distance of 0.8 m. The images of the potted plants of various varieties are presented in Figure 2. A total of 1600 images were captured, with four hundred images obtained for each species.

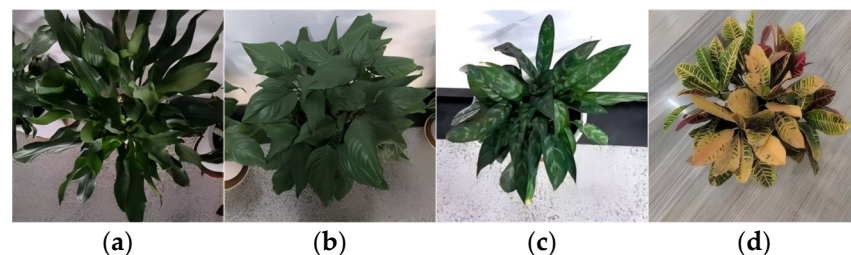


Figure 2. Example of the original image of the dataset. (a) *Rohdea japonica*; (b) *Aglaonema modestum*; (c) *Dieffenbachia seguine*; (d) *Codiaeum variegatum*.

In order to construct an accurate potted plant identification and classification model, it is necessary to augment the original image with data. Offline enhancement allows for the expansion of the number of data samples at one time, which is particularly advantageous for

small-scale datasets. In comparison to online augmentation, there is no longer a necessity to process the images during the training phase [22], which serves to enhance the efficiency of the training process. Accordingly, this study employs offline data enhancement to augment the dataset. In consideration of the image input size of the benchmark model, the original image sizes were reduced to 416×416 in order to align with the model input. As shown in Figure 3, the dataset was tripled to include 4800 images through the utilisation of diverse processing techniques, including image translation, rotation, off-centre rotation, flipping, skewing, and the adjustment of brightness and hue. The dataset was then manually labelled using the Labelme annotation tool and subsequently randomly divided into training, validation, and test sets in a ratio of 7:2:1; the final dataset is shown in Table 1.

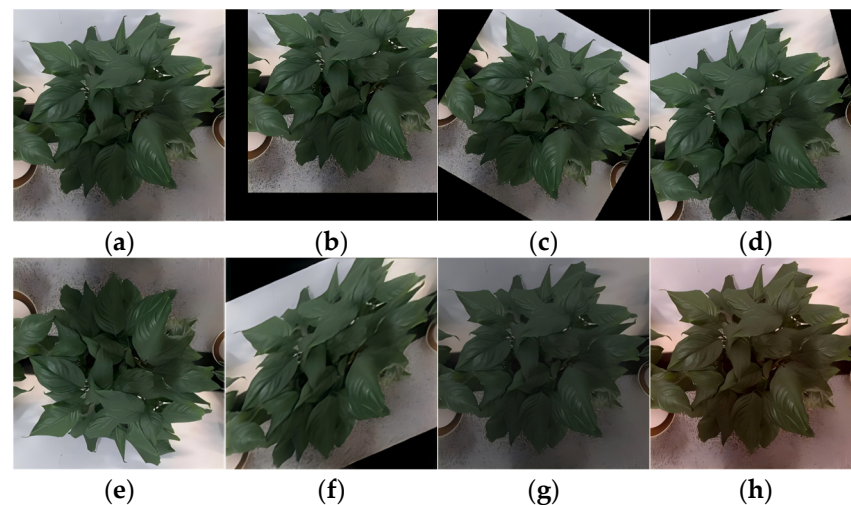


Figure 3. Data offline augmentation methodology (taking *Aglaonema modestum* as an example). (a) Original image; (b) Image translation; (c) Image rotation; (d) Image off-centre rotation; (e) Image flipping; (f) Image skewing; (g) Adjusting brightness; (h) Adjusting colour tones.

Table 1. Dataset for different potted plant varieties.

Class	Train	Validation	Test	Total
<i>Rohdea japonica</i>	840	240	120	1200
<i>Aglaonema modestum</i>	840	240	120	1200
<i>Dieffenbachia seguine</i>	840	240	120	1200
<i>Codiaeum variegatum</i>	840	240	120	1200
Total	3360	960	480	4800

2.1.2. Construction of the Identification and Classification Model of Potted Plants Analysis of the Original YOLOX Nano Network Structure

The YOLOX model builds upon the efficient target detection capability of the YOLO series, incorporating some of the latest advanced detection techniques [23], which enhance its performance in image identification and classification tasks. The YOLOX model employs the YOLOv3 model [24] as the foundational model, substituting a single detection head with a decoupled detection head for classification and regression [25]. Additionally, an IoU branch has been incorporated into the regression branch, resulting in a notable enhancement in both the model's detection accuracy and speed. The YOLOX algorithm employs the anchor-free detection mechanism [26] to directly predict the class and location of the target through each pixel point. This approach circumvents the complex computation and hyper-parameter tuning necessitated by the use of preset anchor frames. The YOLOX model also utilises the SimOTA positive and negative sample allocation strategy [26], which enhances the model's generalisation capability by calculating the pairwise matching degree

of each prediction pair and selecting the top k predictions with the smallest cost in a fixed central region as its positive samples. This approach reduces the computational cost while maintaining efficient training.

The YOLOX Nano model, a modification of the YOLOX series, has the smallest number of parameters of all YOLOX models. It has been demonstrated to have an AP that is 1.8% higher than that of the NanoDet model, which has a comparable number of parameters on the COCO dataset, and 10% higher than that of the YOLOv4-Tiny model [27]. The YOLOX Nano model is able to detect at a higher level of accuracy while reducing computational resource consumption. The network structure is illustrated in Figure 4. In the YOLOX Nano model, the CSP module is based on the concept of CSPNet (Cross Stage Partial Network) [28], which is employed for feature extraction in the backbone and for feature fusion in the neck to ensure the stability of the training process. It performs feature fusion in the form of both CSP1_X and CSP2_X. The backbone of the YOLOX model primarily comprises the Focus module, the DSCBS module, the CSP module, and feature mapping pooling using the SPP module. The Focus module acquires four images with complementary features through a slicing operation on original images. These images are subsequently spliced according to the channel dimension, forming a new feature map. This module enhances the efficiency and accuracy of feature extraction while preventing the loss of information. The CBS is the most fundamental module utilised for extracting features and serves as a pivotal component for feature aggregation and channel expansion. The DSCBS module is an improvement of the CBS module, whereby the conventional convolution is substituted with depthwise separable convolution [29], which significantly reduces the number of parameters and the computational complexity of the model. The SPP (spatial pyramid pooling) module addresses the issue of non-uniformity in input image dimensions through a multi-scale pooling operation [30], enhancing the model's capacity to capture the spatial information of the input image through multi-scale pooling operations.

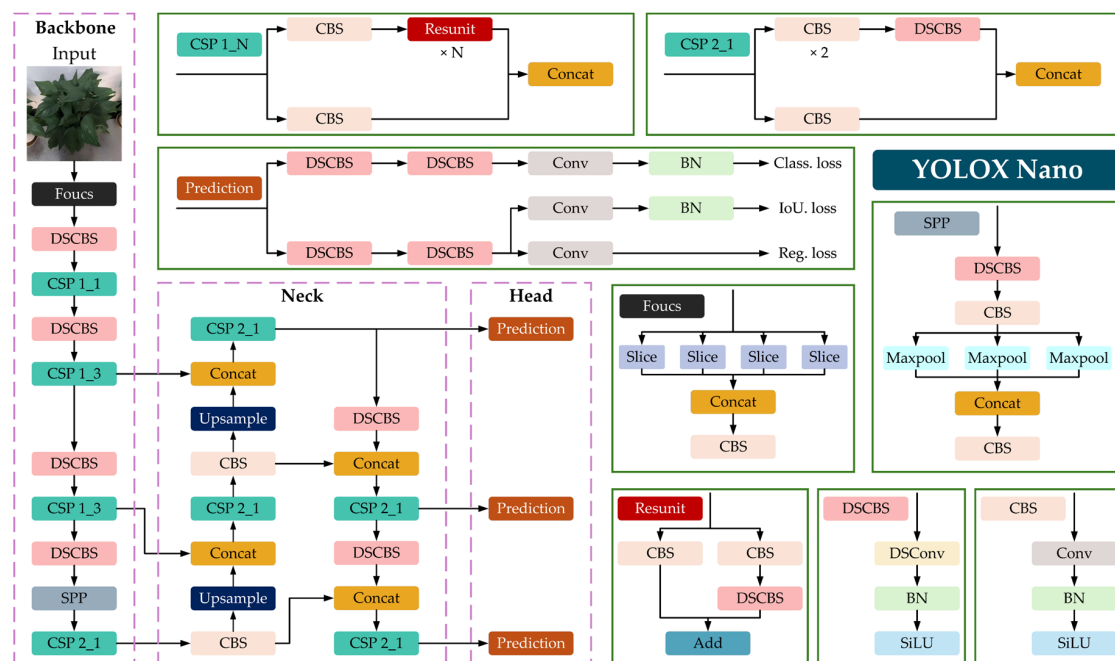


Figure 4. Structure of the YOLOX Nano model.

The Proposed SN-YOLOX Nano-ECA Model

The YOLOX Nano model employs the CSP module for feature extraction in the backbone network, thereby improving the accuracy and efficiency of detection. However, the number of images in the COCO open-source dataset used for the training of the YOLOX Nano model is considerably larger than that of the potted plant dataset constructed in

this paper. Consequently, there may be computational redundancy in the use of the CSP module for feature extraction, which in turn increases the computational complexity and the memory requirement and affects the deployment of the model on embedded devices. In 2018, Megvii (Beijing, China) proposed ShuffleNetV2, a lightweight network architecture for mobile device deployments, and subsequently put forth four practical guidelines for efficient network design [31]. The fundamental unit of ShuffleNetV2 is illustrated in Figure 5a. The channel split operation is introduced in the basic unit, where the input of the feature channel is split into two branches at the beginning of each block. One of these branches undergoes equal mapping, while the other contains three consecutive convolutions. Subsequently, the two branches are connected by the concat operation, and the channel shuffle operation is employed to facilitate information interaction between the two branches. These operations reduce the number of model parameters while maintaining the depth of the model. In the case of the ShuffleNetV2 unit for spatial downsampling, the channel split is negated, each branch undergoes a downsampling operation with a stride of 2, and finally, following the concat process, the feature map space size is reduced by a factor of two while the number of channels is increased by a factor of two. The resulting structure is illustrated in Figure 5b. The ShuffleNetV2 architecture exhibits superior detection accuracy and efficiency compared to lightweight network architectures such as the MobileNet series [32] and GhostNet [33]. In light of the idea of ShuffleNetV2, this study has devised a novel SFB1 module which is capable of efficiently and accurately extracting the multi-scale features of an input potted plant image. Additionally, the SFB2 module was developed for downsampling, with the objective of reducing the size of the feature map and increasing the number of output channels. The retention of more features is achieved through information interaction between the two branches, thereby preventing information loss.

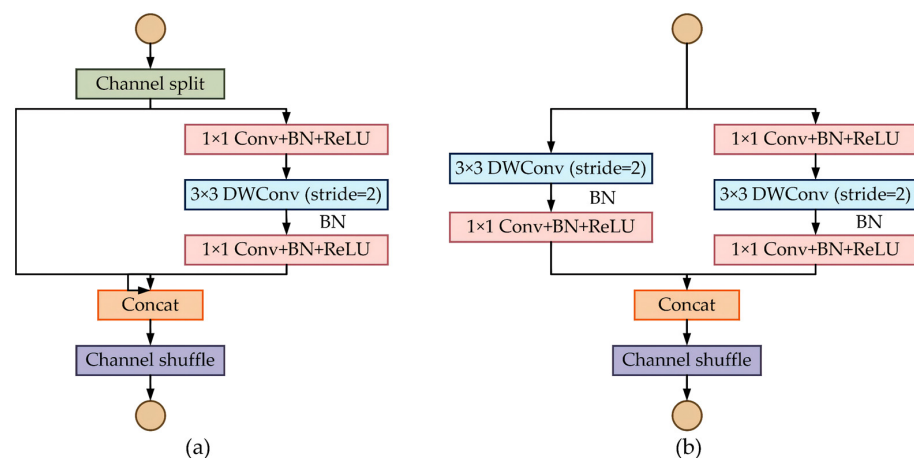


Figure 5. Building blocks of the ShuffleNetV2. (a) Basic unit; (b) Basic unit for spatial down sampling.

It is well established that attention plays a pivotal role in human perception [34]. Indeed, attention mechanisms have been demonstrated to represent a promising avenue for enhancing deep convolutional neural networks (CNNs) [35,36]. The ECA module is a channel attention mechanism that enhances the network's capacity to model image features by dynamically adapting the responses of the different channels. Furthermore, it produces highly accurate detection results with only a few increases in parameters [37]. The principle of the ECA module is illustrated in Figure 6. In this study, we propose the CSP_ECA module, which integrates the ECA attention mechanism into the CSP module in the neck of the model to enhance multi-scale feature fusion and representation. Furthermore, it is integrated into the detection head with the objective of enhancing the deep neural network's representation potential by adaptively adjusting channel weights, allowing greater focus on detected targets while suppressing irrelevant information. Additionally, the ECA module does not reduce the information dimensions, which facilitates the SN-

YOLOX Nano-ECA model's ability to learn the top-level information more efficiently and enhance its classification capabilities for potted plants.

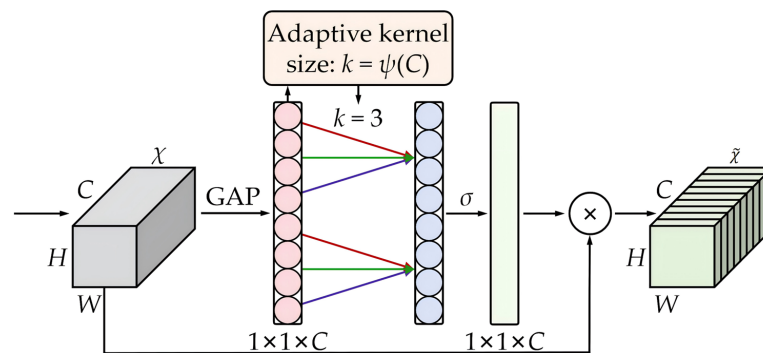


Figure 6. Diagram of the efficient channel attention (ECA) module. Given the aggregated features obtained by global average pooling (GAP), the ECA module generates channel weights by performing a fast 1D convolution of size k , where k is adaptively determined via a mapping of channel dimension C .

The final structure of the SN-YOLOX Nano-ECA model is illustrated in Figure 7. Replacing the DSCBS and CSP modules, the SFB1 and SFB2 modules are employed in the backbone network for the purpose of feature extraction. The Focus module has been removed, and the original image is now processed by the CBRM module. This consists of a basic CBS module for feature extraction in the original input image and a Maxpool module that retains the key information in the feature map and enhances the feature representations while reducing the feature map size to reduce the computational costs. Furthermore, the SPP module has been removed. Meanwhile, the CSP module has been replaced with the CSP_ECA module, incorporating the attention mechanism at the neck of the model. A new detection head enhanced by the ECA module has also been implemented.

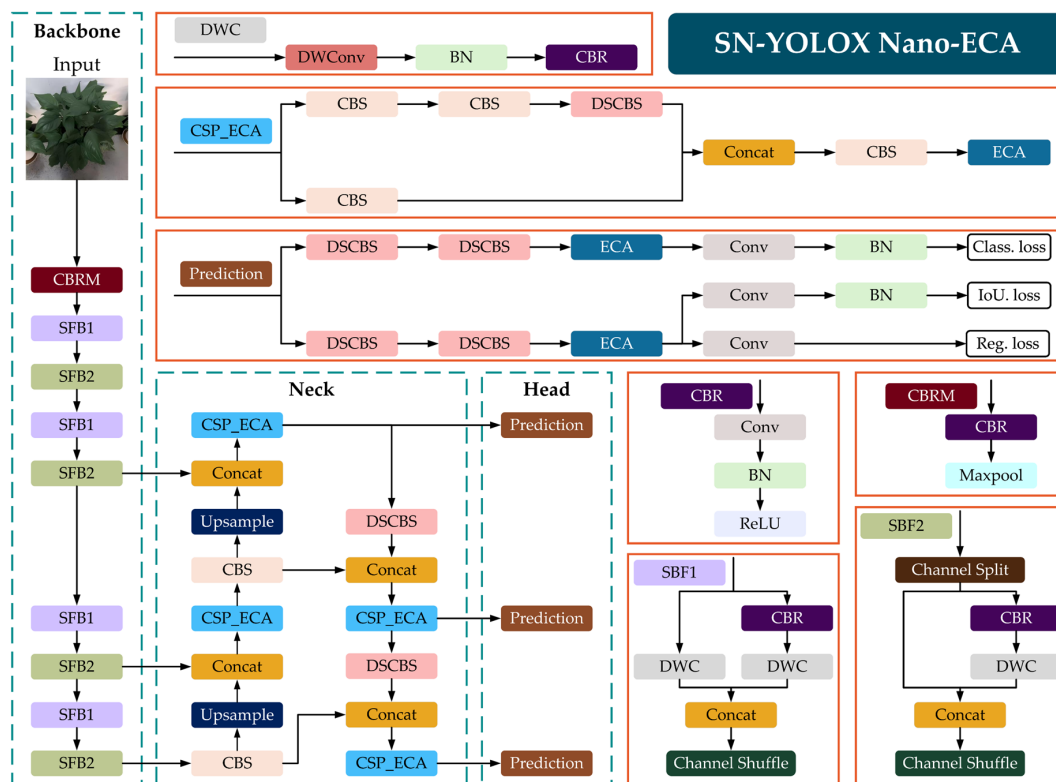


Figure 7. Structure of the proposed SN-YOLOX Nano-ECA model.

2.1.3. Model Evaluation Metrics

This study employs a range of metrics to evaluate the performance of different network models on the dataset, including accuracy (A), precision (P), recall (R), $F1$ -score, mean average precision (mAP), frames per second (FPS), and floating-point operations ($FLOPs$) [38].

The accuracy of a model is defined as the proportion of all samples that are correctly predicted by the model. This can be calculated using the following equation:

$$Accuracy = \frac{TP + TN}{TP + FP + TN + FN} \quad (1)$$

where TP represents the correctly identified positive classes, TN represents the correctly identified negative classes, FP represents the incorrectly identified negative classes, and FN represents the incorrectly identified positive classes.

As shown in Equation (2), precision represents a measure of the proportion of samples predicted to be positive that are actually positive. This is employed to assess whether the model is capable of accurately identifying the target.

$$Precision = \frac{TP}{TP + FP} \quad (2)$$

As shown in Equation (3), recall is the proportion of correctly predicted positive samples out of all actually positive samples, reflecting the model's ability to identify all positive samples.

$$Recall = \frac{TP}{TP + FN} \quad (3)$$

The mean average precision (mAP) represents the average of the detected average precision (AP) across all target categories. It is used to measure the precision and recall of the model on different categories and reflects the overall performance of the model. The intersection over union (IoU) is employed in target detection tasks to assess the degree of overlap between the predicted box and the real box. In this paper, the IoU threshold is set to 0.5, with $mAP_{0.5}$ employed for assessing the comprehensive identification and classification efficacy of the model, as shown in Equation (4).

$$mAP_{0.5} = \frac{1}{n} \sum_{i=1}^n AP_i \times 100\% \quad (4)$$

Here, n is the number of categories and AP_i is the average precision of category i when the IoU threshold is 0.5.

The $F1$ -score represents the reconciled mean of precision and recall, which balances the two metrics for a comprehensive evaluation of the model. This is calculated in accordance with Equation (5).

$$F1\text{-score} = \frac{2 \times Precision \times Recall}{Precision + Recall} \quad (5)$$

The frames per second (FPS) is used to denote the number of images that are detected per second, which reflects the speed at which the model is able to detect images. The floating point operations ($FLOPs$) metric is used to evaluate the complexity of the model.

2.1.4. Experiment Conditions

The computer configurations employed for the purposes of training, validating, and testing the model in this study comprise an Intel® Core™ i9-14900HX (Santa Clara, CA, USA) with 24 cores and a selected NVIDIA GeForce RTX 4070 (Santa Clara, CA, USA) laptop GPU with 8 GB of video memory, 32 GB of RAM, and a Windows 11 system. The programming tool employed was PyCharm, utilising the Python 3.11.5 programming

language. The deep learning framework was Pytorch 2.1.1, with CUDA 12.2 employed for the acceleration of training processes.

All network models underwent training utilising pre-trained weights provided by the model authors. The same data pre-processing and augmentation method was used for all test models. In order to achieve rapid training without any loss of accuracy, the batch size was set to 16. To guarantee model convergence, the model was trained for 200 epochs. The input was an RGB image 416×416 pixels in size in the JPEG format. The SGD optimiser with a momentum factor of 0.937 was selected with an initial learning rate of 0.01, a final learning rate of 0.001, and a weight decay factor of 0.0005. The training set was employed for the training of the model parameters, the validation set was utilised for the ablation experiments and comparisons with other models, and the test set was used for comparisons with the classification results of the human eye.

2.2. Foliar Fertiliser Spraying Methods

2.2.1. Phenotypic Information Acquisition

Edge Contour Extraction

In real-time image detection scenarios, a considerable amount of invalid information is present in the collected target plant images, including the background, noise, and other plant-related interference. Consequently, removing interference, segmenting the target and background, and accurately extracting the edge contour of the target plant are essential prerequisites for the acquisition of accurate phenotypic information.

Prior to edge contour extraction, the captured image is subjected to a degree of pre-processing. The process of converting a colour image, which contains three channels of information, into a grayscale image, which contains only one channel of information, has the effect of reducing the difficulty of subsequent image data processing. The filtering of a grayscale image can effectively remove the noise and smooth the contour edges, thereby facilitating the extraction of target feature information. The most commonly employed filtering methods are median filtering, mean filtering, and Gaussian filtering [39]. Gaussian filtering is an effective method for suppressing noise while maintaining the smoothness of contour edges and preserving detail information in a more comprehensive manner. Accordingly, the Gaussian filter was employed for the preliminary processing stage of edge contour extraction.

The Otsu adaptive threshold segmentation algorithm was employed to segment the filtered image, thereby separating the target individual plants from the irrelevant background. The morphological processing methods of opening and closing operations were employed to clarify the characteristics of image information further, thereby rendering the edge contour more clear and facilitating its extraction. The most commonly used algorithms for edge detection and contour extraction include Sobel, Prewitt, and Canny, etc. [40]. The Canny algorithm employs a series of operations, including noise removal, calculation of the gradient, non-maximum value suppression, double threshold detection, and others, to connect strong and weak edges through the removal of noise and the calculation of gradients, which allows for the accurate detection of edges. This study used this method for edge extraction. The results of the edge contour extraction process for the potted plants are shown in Figure 8.

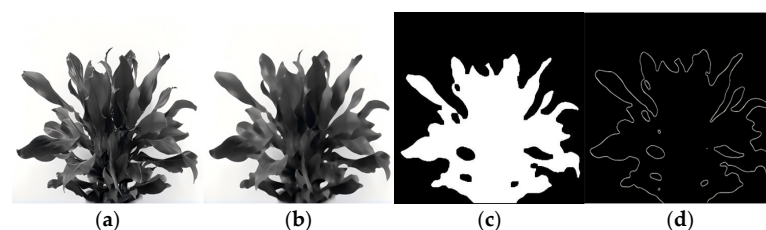


Figure 8. Potted plant edge contour extraction process. (a) Image graying; (b) Gaussian filtering; (c) Segmented image; (d) Canny operator.

Plant Leaf Area and Height Information Acquisition

The leaf area is a significant piece of phenotypic information, reflecting the growth status of potted plants [41] and influencing the decision-making on the spraying amount. The height of the plant serves to determine the positioning and targeting of the actuator of the spraying robot. It is therefore essential to investigate the methodology for acquiring data on plant height and leaf area based on the target plant's edge contour. In order to ascertain the area of the leaves, the number of pixels enclosed within the edge contour is calculated on the basis of the results of the image segmentation. The leaf area coefficient (L_{ac}) is defined as the basis for the decision-making on the amount of foliar fertilizer sprayed, representing the ratio of the area of the plant edge contour to the area of the image. This is calculated in accordance with Equation (6).

$$L_{ac} = \frac{S_{Ta}}{S_{Ta} + S_{Ba}} \times 100\% \quad (6)$$

Here, S_{Ta} is the number of pixel points within the target edge contour area and S_{Ob} denotes the number of pixel points within the target external background area. Figure 8b illustrates the leaf area data obtained through this methodology. The real leaf area (S_r) is calculated using Equation (7).

$$S_r = S_v \cdot L_{ac} \quad (7)$$

Here, S_v represents the real viewpoint range of the captured image, which is $0.8 \text{ m} \times 0.8 \text{ m}$ in this paper. The obtained leaf area information is shown in Figure 9b.

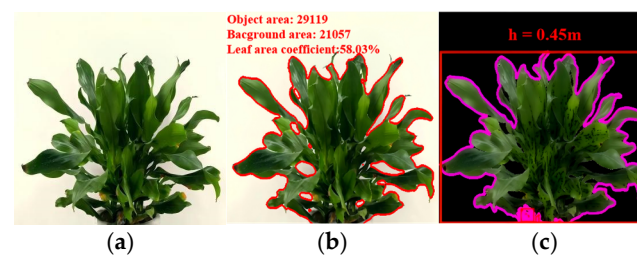


Figure 9. Acquisition of phenotypic information. (a) Individual image; (b) Leaf area information; (c) Plant height information.

In order to ascertain the height information, it is first necessary to calculate the convex packet that exists on the edge contour. The next step is to find the smallest bounding rectangle on the convex packet, which enables the smallest anchor frame to be identified. The size information of this anchor frame can then be mapped to the manual measurements, as illustrated in Figure 9c, in order to obtain the height and the centre position information of the plant canopy.

2.2.2. Decision-Making for Spraying Operations

Figure 10 illustrates the decision-making process for the application of foliar fertiliser. The real-time collected individual images of potted plants are subjected to preprocessing in order to perform image segmentation and extract edge contours. Subsequently, phenotypic information, including the plant height and leaf area, is obtained. The growth state of the plant is classified according to the leaf area, thus enabling decision-making concerning the amount of foliar fertilizer sprayed. The positioning of the spray nozzles is determined according to the information obtained regarding the height of the plants. The height and angle of each nozzle are adjusted in order to align them with the centre of the plant canopy from both the front and the reverse side of the leaves, thereby enabling decision-making concerning the dual-face target spraying for foliar fertiliser.

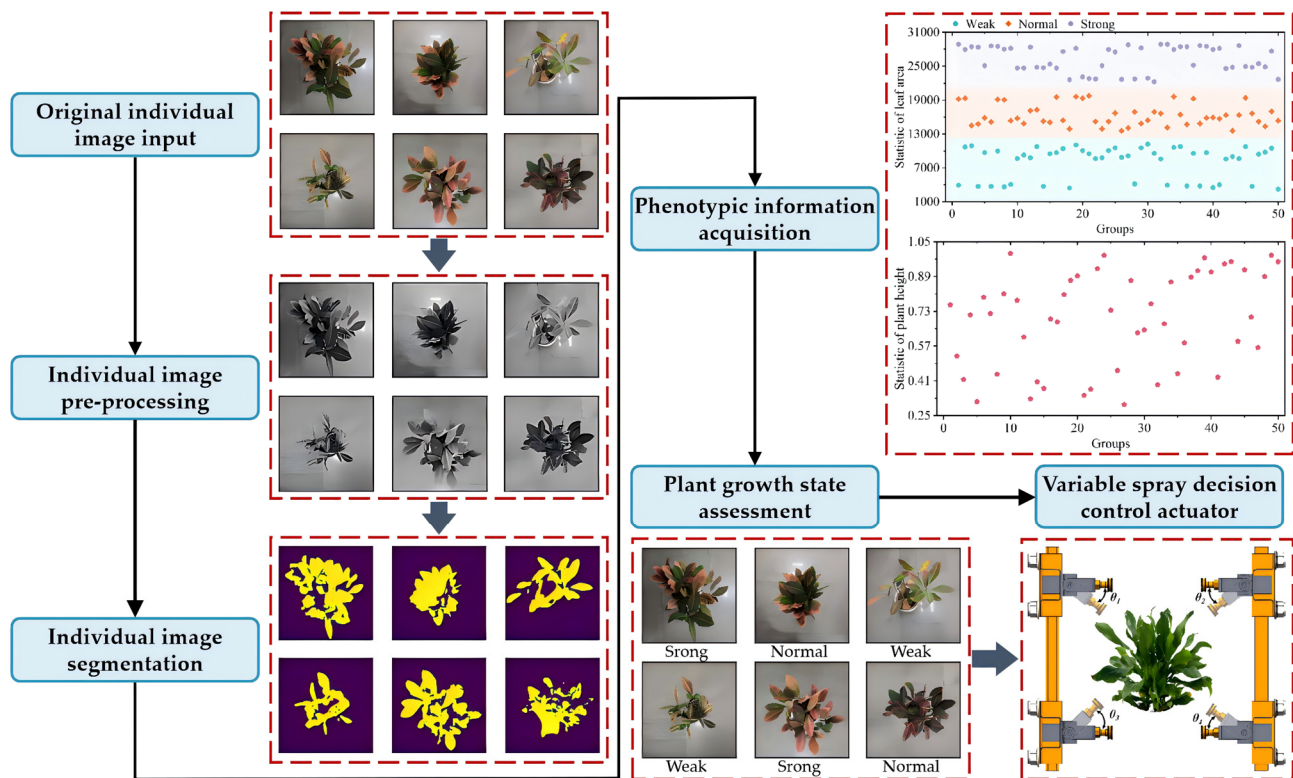


Figure 10. Decision process for foliar fertiliser with dual-face target precision variable spraying.

Decision-Making on the Amount of Foliar Fertiliser Sprayed

The amount of foliar fertiliser applied is directly influenced by the plant leaf area, which determines the precise fertiliser requirement and serves as the basis for variable spraying [42]. The leaf area size reflects the plant's ability for autonomous photosynthesis. The application levels of fertiliser required by plants exhibiting different growth states must be adjusted in order to meet their respective reasonable nutrient requirements. In this study, the leaf area coefficient proposed in Equation (8) was employed to categorise the growth status of plants into strong, normal, and weak categories. Strong plants have a large leaf area, enabling them to synthesise sufficient nutrients through photosynthesis to meet their growth requirements. Weak plants, on the other hand, need external fertiliser to assist them in obtaining nutrients to thrive due to their small leaf area. Normal plants with a moderate leaf area can be sprayed with an intermediate level of foliar fertiliser. The four potted plants selected for this study exhibited comparable leaf growth patterns in each growth status. Preliminary tests indicated that the plant growth stages could be classified using the identical standard leaf area coefficient. Additionally, the foliar fertiliser spraying amount coefficient (S_{ac}) was determined based on the growth status to further determine the amount of foliar fertiliser sprayed. The classification of growth status and L_{ac} , along with the S_{ac} , is presented in Table 2.

The foliar fertiliser used in this study was a composite foliar fertiliser ($N:P_2O_5:K_2O = 28:12:13$), comprising amino acids, biologically active substances, and essential microelements for plant growth. It can aid weak seedlings in becoming strong and enhance the growth of leaves. The standard spraying amount, A_{S_i} , under the current growth status was calculated using the average plant canopy volume as a benchmark, based on the amount applied per hectare, the plant spacing, and row spacing. The final spray amount of the foliar fertiliser required for the target plant was calculated as A_i based on the spray amount coefficients determined by the growth status. Relevant equations are presented in Equations (8)–(10).







$$A_{s_i} = \frac{M \cdot R_s \cdot P_s \cdot V_{C_i}}{10000 \cdot V_{Ca}} \times 100\% \quad (8)$$

$$V = \frac{2}{3} \times S_r(h_2 - h_1) \quad (9)$$

$$A_i = S_{ac_i} \cdot V_{S_i} \quad (10)$$

Here, M , R_s , and P_s are the amount of foliar fertiliser applied per hectare (kg/hm^2), row spacing (m), and plant spacing (m), respectively; V_{Ca} and V_{C_i} denote the mean value of plant canopy volume and the volume of the target plant canopy with the growth status of class i , respectively. The shape of the canopy of the potted plant was a semi-ellipsoid with a rounded base, and the foliar fertiliser spraying amount was determined based on the volume of the region (V), which was calculated in accordance with the methodology outlined in Equation (9). In this equation, h_1 and h_2 represent the height of the top and bottom of the canopy, m, respectively. Additionally, S_{ac_i} is the foliar fertiliser spraying amount coefficient for potted plants of class i growth status.

Table 2. Classification of plant growth status and division of parameters for spraying operations.

Image Segmentation Results		L_{ac} (%)	Growth Status	S_{ac}
		≤ 30	Weak	1.2
		30~60	Normal	1.0
		≥ 60	Strong	0.8

Decision-Making on the Dual-Face Target Spraying for Foliar Fertiliser

Therefore, accurately positioning the spraying apparatus based on the plant height information is a prerequisite for the dual-face target precise application of foliar fertiliser [43]. As illustrated in Figure 11a, the operational heights of the nozzles on the left and right were determined based on the acquired data regarding the height of the plants. The heights h_1 , h_2 , h_3 , and h_4 were calculated to ensure that the plant was situated at the centre of the upper and lower nozzles at the specified spatial heights, which guaranteed that the front and reverse side of the leaves were able to receive foliar fertiliser spraying. Subsequently, the rotational angles θ_1 , θ_2 , θ_3 , and θ_4 for each nozzle were calculated to align with the center of the canopy according to their relative positions, as shown in Figure 12b. This allowed for precise dual-face spraying of foliar fertiliser on the target. On the one hand, the dual-face spraying of foliar fertiliser onto the front and reverse side of the leaves simultaneously can enhance the absorption efficiency of the foliar fertiliser by the leaves. On the other hand, the spraying of foliar fertiliser at the centre of the plant canopy can prevent the fertiliser droplets from falling directly outside the canopy, thereby enhancing the utilisation rate of foliar fertiliser and reducing wastage.

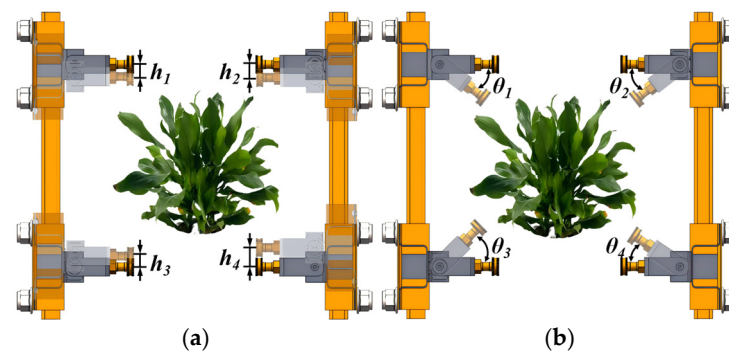


Figure 11. Precise positioning process of the spray nozzles. (a) Spray nozzle height adjustment process; (b) Spray nozzle angle adjustment process.

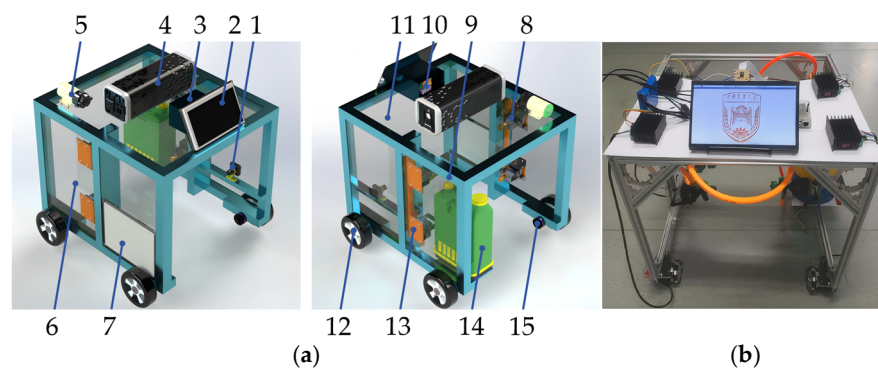


Figure 12. Efficient robot platform for dual-face target precision variable spraying of foliar fertiliser. (a) Overall structure: (1) CCD camera; (2) Teach pendant; (3) Control box; (4) Power supply; (5) pump; (6) Side plate; (7) Backdrop; (8) Adjustable spray nozzle; (9) Rack; (10) Embedded controller; (11) Cover plate; (12) Moving wheel; (13) Slide for nozzle position adjustment; (14) Fertiliser tank; (15) Mobile motor; (b) Real test prototype.

2.3. Robotic Platform for Dual-Face Target Variable Spraying of Foliar Fertilisers

2.3.1. Overall Structure

This study proposes an efficient computer vision-based foliar fertiliser dual-face target accurate variable spraying robotic platform, integrating the SN-YOLOX Nano-ECA model for real-time identification and classification of potted plants and Section 2.2. The overall structure of the robotic platform is shown in Figure 12a, which includes a frame, moving wheels, a charge-coupled device (CCD) camera, a teach pendant, adjustable nozzles, a fertiliser tank, and a core controller, etc. Among them, the nozzle selected was the 110015-type fan-shaped anti-dripping nozzle (produced by Hebei Shuangheng Agricultural Machinery, Xingtai, China). The platform passed over the potted plant during operation, and CCD camera collected images in real time. Upon detecting the plant, the travelling wheel stops. The deployed classification model and phenotypic information acquisition algorithm calculates the category and phenotypic information of the target plant and displays them on the teach pendant. Concurrently, the core controller controls the height and angle of the adjustable nozzles and the switch-on time of the pumps, so that the nozzles are able to carry out precise and quantitative spraying on the target. In order to enhance the efficiency of the spraying process, the four nozzles are partitioned into two categories based on the disparate orientations of the sprayed leaves, and each category employs one solenoid valve to regulate the switching of the pump, thereby ensuring the synchronism of the nozzles' operation. The prototype constructed for tests is illustrated in Figure 12b.

The robot platform can be divided into four modules according to their functions, as shown in Figure 13. The composition of these modules allows the robot to meet the operational requirements of the various segments of foliar fertiliser spraying, as demonstrated in Figure 14. The NVIDIA Jetson Orin Nano serves as the core controller, responsible for

processing the input positioning data and real-time image information and subsequently generating control signals for the robot platform's navigation and operational commands. This enables the integration and coordination of the various modules and realizes the autonomous operation of foliar fertiliser spraying. The accurate deployment of the potted plant real-time identification and classification model and the precise positioning and navigation of the robot platform are prerequisites for the system to accurately carry out the decision-making of foliar fertiliser variable spraying. This has a direct impact on the performance of the foliar fertiliser dual-face target precision variable spraying robotic system.

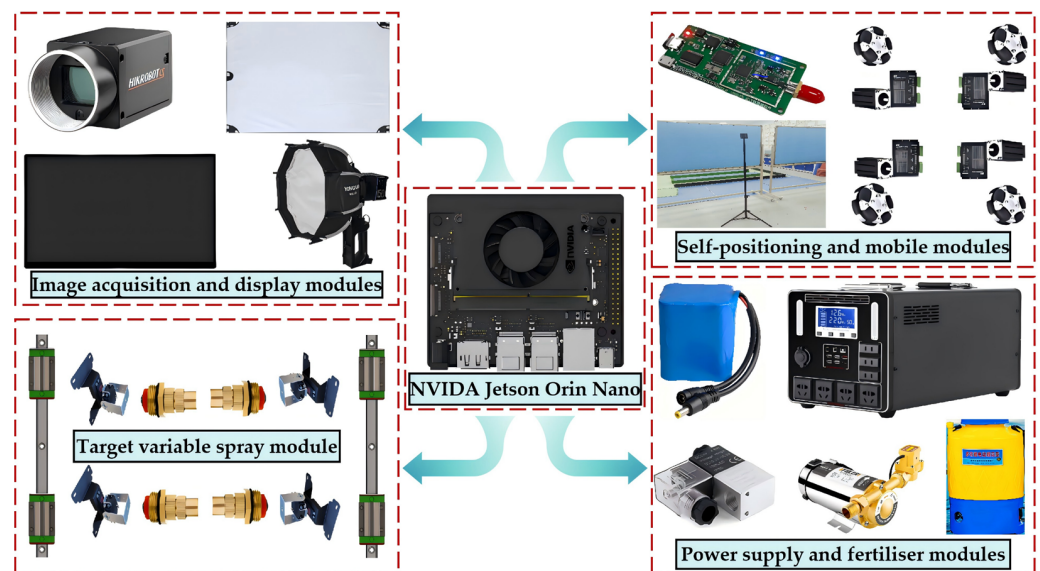


Figure 13. Foliar fertiliser dual-face target precision variable spraying robot platform composition.

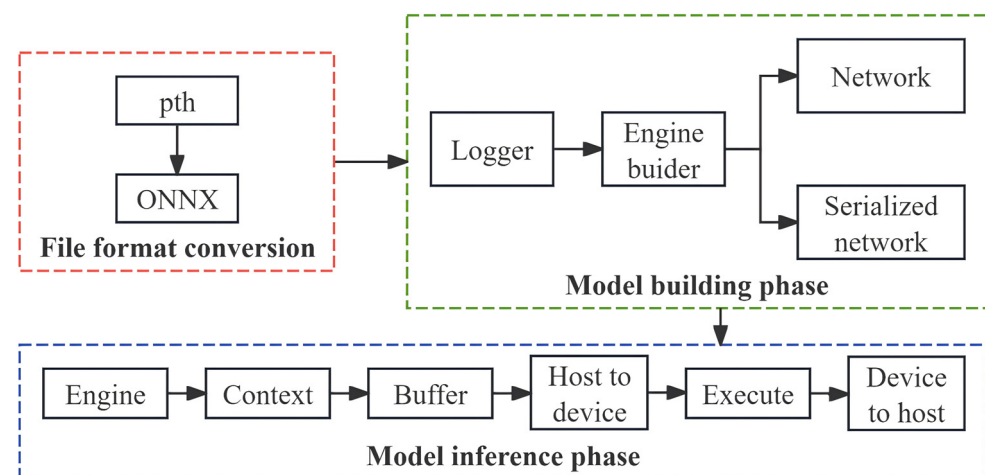


Figure 14. Workflow for model deployment.

2.3.2. Deployment of a Target Identification and Classification Model for Potted Plants

The training of models is typically conducted on powerful GPU workstations, yet their deployment occurs on embedded devices that are more susceptible to fluctuations in computational resources during practical applications. This presents a significant challenge to the real-time inference efficiency of the models.

In this study, the edge computing platform NVIDIA Jetson Orin Nano was selected for model deployment and inference. It employs the Ampere GPU architecture with various standard hardware interfaces and offers the advantages of high performance, low energy consumption, and a compact form factor. This means it is widely used in the field of

robotics. TensorRT is a high-performance inference engine developed by NVIDIA for the acceleration of deep learning inference which can provide low-latency and high-throughput deployment of inference. In this study, TensorRT 10.2 is employed for the deployment of the model on the NVIDIA Jetson Orin Nano, with data quantification undertaken in order to accelerate the inference process of the potted plant target detection and classification model. The specific deployment flow of the model is illustrated in Figure 14.

2.3.3. Autonomous Positioning and Navigation Methods

Beacon positioning using the received signal strength indicator (RSSI) is a Bluetooth-based technique [44] widely employed for accurate indoor positioning and navigation. This study constructs a five-beacon RSSI positioning and navigation system in a laboratory environment, consisting of four stationary beacons and one mobile beacon on the robot platform. The positioning principle is shown in Figure 15. Each beacon continuously transmits wireless signals, and the Bluetooth module on the robot platform calculates the distance to each beacon based on the RSSI from different beacons. The relationship between signal strength and distance can be expressed by the shadowing signal propagation model, as shown in Equations (11) and (12).

$$p = p_0 + 10n \log_{10} \left(\frac{d}{d_0} \right) + \zeta \quad (11)$$

$$RSSI = p_0 - p \quad (12)$$

Here, p and p_0 are the signal strengths at the pending location and at a distance (d_0) from the signal source, dBm, respectively; d and d_0 represent the distance from the pending location to the signal source and the reference distance, m, respectively; n is the path loss factor; and ζ is the masking factor.

The system acquires the position coordinates and speed information of the robot platform by monitoring the distance between the mobile beacon and the stable beacon. It then employs a differential control to adjust the direction and the speed of the robot platform in accordance with the pre-set end position, thereby enabling autonomous navigation and movement. Concurrently, the system corrects any positioning and moving errors in motion in real time based on the difference principle, thereby ensuring the accuracy of the robot platform's positioning and navigation.

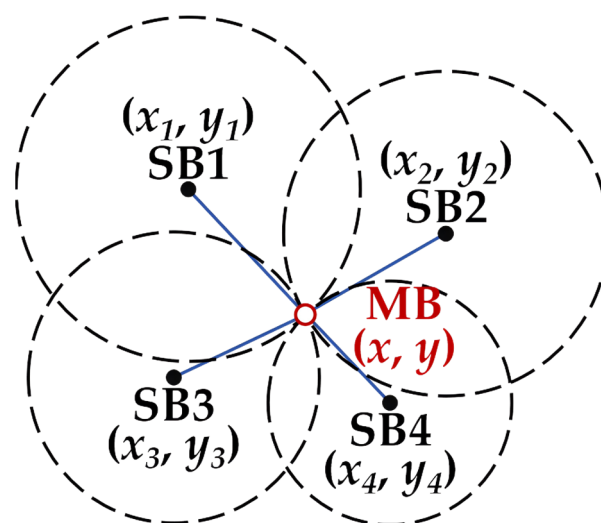


Figure 15. Principle of the five-beacon positioning system. SB1, SB2, SB3, and SB4 represent the stationary beacons; MB represents the mobile beacon.

3. Results

3.1. Assessment of the Effectiveness of Identification and Classification of Potted Plants

3.1.1. Results of Ablation Experiments

In this paper, YOLOX Nano was used as the base model, and the efficacy of each enhancement was ascertained through ablation experiments. The models underwent training and testing utilising an identical dataset. The model classification effect and the computational cost and speed for the ablation experiments are shown in Tables 3 and 4. It can be observed that the ShuffleNetV2 exhibits inferior performance compared to YOLOX Nano. Following the replacement of the backbone network with ShuffleNetV2, the accuracy, precision, recall, *F1-score*, and *mAP* were augmented by 2.13%, 1.66%, 1.64%, 1.95%, and 1.57%, respectively, in comparison to the YOLOX Nano. Concurrently, the *FLOPs* and parameters were reduced to 0.14 G and 0.45 M, respectively, while the detection *FPS* was elevated to 677.3. The incorporation of the ECA module into the model neck and head resulted in a notable enhancement in performance, with the accuracy, precision, recall, *F1-score*, and *mAP* reaching 96.18%, 98.83%, 95.59%, 97.18%, and 97.42%, respectively. Concurrently, the model *FLOPs* and the number of parameters exhibited increases of merely 0.02 G and 0.03 M, respectively. The detection *FPS* experienced a decline, but remained at an acceptable level of 659.5. This demonstrates that the incorporation of the ECA module significantly improves the classification ability for potted plants with only a very small additional computational cost and efficiency. Overall, enhancements to YOLOX Nano improved classification performance and efficiency by reducing parameters and computational complexity.

Table 3. The results concerning classification efficacy in the ablation experiments.

Model	YOLOX Nano	ShuffleNetV2	ECA	A (%)	P (%)	R (%)	F1-Score (%)	mAP (%)
1	on	\	\	92.50	94.67	92.57	93.6	94.89
2	\	on	\	90.38	91.91	90.54	91.22	94.63
3	on	on	\	94.71	96.72	94.21	95.46	96.46
4	on	on	on	96.18	98.83	95.59	97.18	97.42

Note: “on” indicates that the section has been added to the network model; “\” indicates that the section has not been added to the network model; Model 1, 2, 3, and 4 represent YOLOX Nano, ShuffleNetV2, SN-YOLOX Nano, and SN-YOLOX Nano-ECA, respectively.

Table 4. The results concerning computational cost and speed in the ablation experiments.

Model	YOLOX Nano	ShuffleNetV2	ECA	FLOPs (G)	Parameters (M)	FPS
1	on	\	\	1.12	0.99	495.3
2	\	on	\	0.26	0.77	560.6
3	on	on	\	0.14	0.45	677.3
4	on	on	on	0.16	0.48	659.5

Figure 16 illustrates the trend in the accuracy of the ablation experiments. As the number of training rounds increased, the accuracy of all models showed an upward trend, peaking and stabilising at 200 epochs. The ShuffleNetV2 model exhibited the poorest performance, with a slow convergence of the model and a lower model accuracy after stabilisation. The remaining models showed rapid convergence during training. Among them, the SN-YOLOX Nano-ECA model demonstrated significant improvement in the early stages, followed by gradual enhancement and stabilisation at a high level as training epochs increased, achieving the best performance among all models.

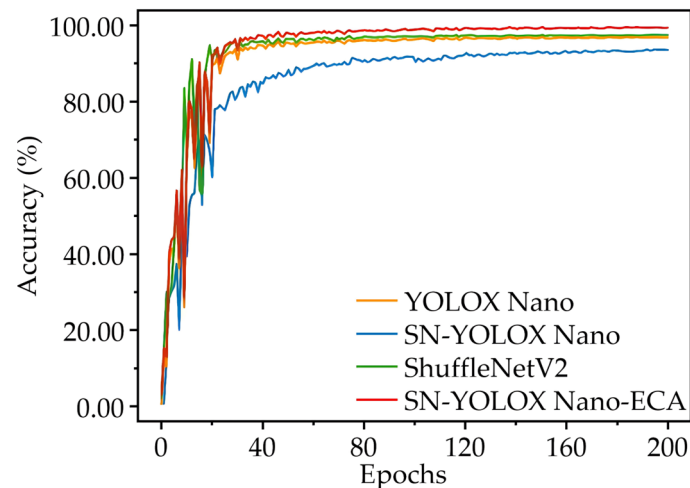


Figure 16. Accuracy change curves during training in ablation experiments.

3.1.2. Comparison of Different Models

The SN-YOLOX Nano-ECA model was compared with the classical convolutional neural networks (CNNs) VGG16 [45] and ResNet50 [46] and the classical lightweight CNNs MobileNetV3 [32], GhostNet [33], and YOLOv5s in the potted plant classification task. For the four potted plant categories, the number of neurons in the last fully connected layer was set to four for all models under comparison, while all other parameters were fixed in order to ensure the reliability of the experimental results. The model was trained using the same dataset and strategy, and the optimal weight parameters were then saved. Subsequently, the model was tested on the same test set.

The classification performance of each model on the validation set and the loss variation curves are presented in Table 5 and Figure 17, respectively. The model loss value essentially reached stability at 200 epochs. Among the classical CNNs, VGG16 exhibited inferior performance relative to ResNet50. VGG16 demonstrated accuracy and precision values of 88.44% and 90.25%, respectively, and exhibited slow convergence. This may be attributed to the fact that the relatively high learning rate (0.01, 0.001) employed to facilitate rapid model convergence is not optimal for VGG16 with a substantial number of parameters. In comparison, ResNet50 showed excellent classification performance, with an accuracy and precision of 95.92% and 96.21%, respectively. Among the classical lightweight CNNs, MobileNetV3 and GhostNet exhibited inferior classification performance, yet still outperformed VGG16. Conversely, the single-stage target detector YOLOv5s demonstrated remarkable proficiency, with 94.75% accuracy and 97.34% precision, even surpassing that of ResNet50. The size and computational cost of lightweight CNNs are significantly lower than those of CNNs, and with high classification speed, they are capable of performing the target classification task effectively and are easily deployable on embedded devices. In comparison to the above network models, the SN-YOLOX Nano-ECA model demonstrated a rapid convergence speed and stable performance, with an average accuracy, precision, and recall of 96.18%, 98.83%, and 95.59%, respectively, and a classification speed of 659.5 FPS. This makes it suitable for deployment on embedded devices to complete the task of real-time classification of potted plants. Furthermore, its FLOPs and parameters are only 0.16 G and 0.48 M, indicating low resource demand for model deployment on the computing platform, which enhances deployment efficiency.

Table 5. Comparison of different models' performance on the validation set.

Model	A (%)	P (%)	R (%)	F1-Score (%)	mAP (%)	FLOPs (G)	Parameters (M)	FPS
VGG16	88.44	90.25	97.63	92.70	90.37	14.42	126.73	102.5
ResNet50	95.92	96.21	93.61	94.89	96.85	4.16	23.56	164.6
MobileNetV3	88.76	93.33	90.30	91.86	93.22	0.23	4.23	534.8
GhostNet	91.79	92.47	92.13	92.31	94.48	0.15	3.89	596.5
YOLOv5s	94.75	97.34	93.96	95.71	97.09	16.34	7.12	462.1
SN-YOLOX Nano-ECA	96.18	98.83	95.59	97.18	97.42	0.16	0.48	659.5

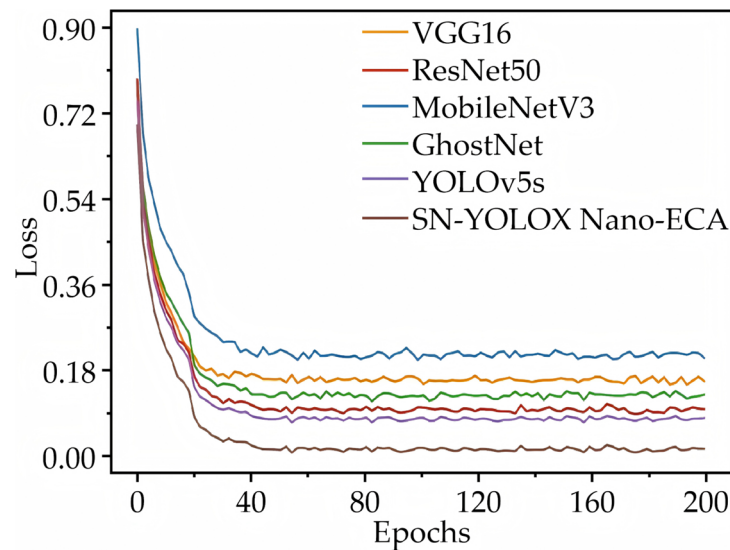


Figure 17. Loss change curves of different models on the validation set.

The results on the training and validation sets are not indicative of the model's actual performance and are mainly used to select optimal hyperparameters for training. To further compare the performance of SN-YOLOX Nano-ECA with classical CNNs and lightweight CNNs, the model was tested on the test set. The confusion matrix for the classification results is presented in Figure 18. The YOLOv5s model achieved the best classification performance among lightweight CNNs, while ResNet50 demonstrated superior performance among classical CNNs. The classification results of VGG16 for potted plants were the least accurate among all the models tested and did not meet the classification requirements of this study. The SN-YOLOX Nano-ECA model had the best effects for classifying all four potted plants. Furthermore, all models demonstrated a greater capacity to classify *Rohdea japonica* and *Codiaeum variegatum* than *Aglaonema modestum* and *Dieffenbachia seguine*. This may be due to *Rohdea japonica*'s more slender leaf shape, which is a distinctive characteristic, compared to the other three potted plants. *Codiaeum variegatum* is characterised by yellow-green leaves with yellow stripes and spots, which are readily distinguishable. The leaf colours and shapes of *Aglaonema modestum* and *Dieffenbachia seguine* are similar, although *Dieffenbachia seguine* exhibits irregular white markings. However, this marking is unevenly distributed and less obvious, and different lighting conditions might adversely affect the display of the mottling pattern in the captured images of the plants. The SN-YOLOX Nano-ECA model achieved similar classification results on the four potted plants, which indicates that the proposed model is more effective in extracting small differences between similar targets, mitigates external environmental influences, and demonstrates excellent generalisation ability.

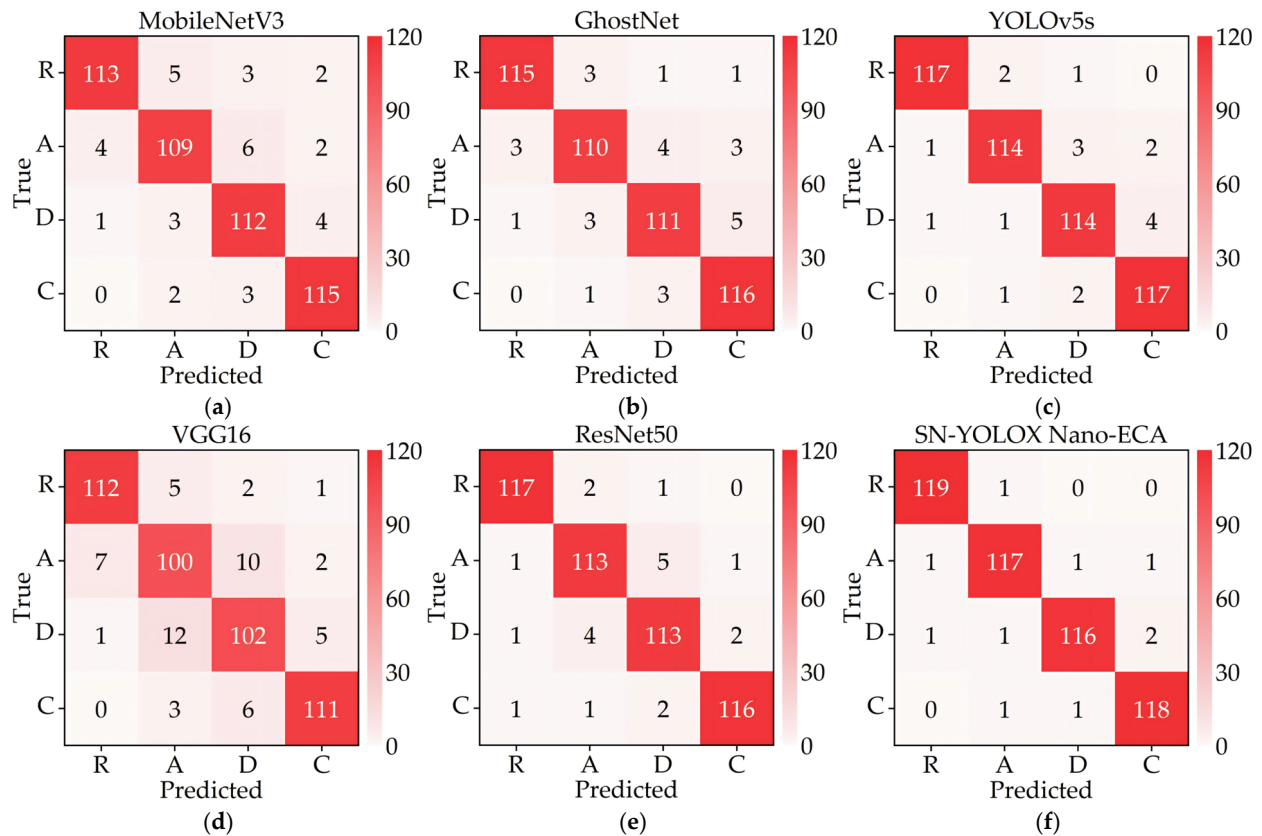


Figure 18. Confusion matrix for classification results for potted plants with different models. (a) MobileNetV3; (b) GhostNet; (c) YOLOv5s; (d) VGG16; (e) ResNet50; (f) SN-YOLOX Nano-ECA. Note: R, A, D, and C represent *Rohdea japonica*, *Aglaonema modestum*, *Dieffenbachia seguine*, and *Codiaeum variegatum*, respectively.

3.2. Results of Phenotypic Information Acquisition

The system makes foliar fertiliser spraying decisions based on the phenotypic information of potted plants, thus making it crucial to ensure the accuracy of this information. Images of 10 potted plants were randomly selected for the purpose of extracting information regarding leaf area and plant height, and the resulting data was then compared with the actual measurement results. The true plant height was obtained through manual measurement, while the true leaf area was determined by manually extracting the number of pixels in the area covered by the leaves in the image. The evaluation metrics were leaf area precision (L_{ap}) and plant height precision (P_{hp}), which were calculated in accordance with the formulas presented in Equations (13) and (14).

$$L_{ap} = \left(1 - \left| \frac{L_{ea} - L_{ta}}{L_{ta}} \right| \right) \times 100\% \quad (13)$$

$$P_{hp} = \left(1 - \left| \frac{P_{eh} - P_{th}}{P_{th}} \right| \right) \times 100\% \quad (14)$$

Here, L_{ea} and L_{ta} are the extracted and true measured leaf areas, expressed as the number of pixels, and P_{eh} and P_{th} are the extracted and true measured plant heights, expressed, m.

The results of the experimental tests are presented in Table 6. The extracted leaf area and plant height were smaller than the actual measurements, likely due to information loss at the edges during contour extraction, which reduces the image contour. Furthermore, the precision of leaf area extraction for potted plants reached above 97%, while the precision of plant height extraction was above 96%. Notably, the leaf area extraction precision was

slightly higher than the plant height extraction precision. This discrepancy can be attributed to the narrower edge regions of the leaves at the top of the plant canopy, making pixel points in this area susceptible to disappearance during contour extraction. Consequently, the extracted contour may exhibit a greater degree of shortening in the direction of the plant canopy, leading to a larger underestimation of plant height. In general, the extracted leaf area and height information of potted plants is precise and meets the criteria for foliar fertiliser spraying decisions.

Table 6. Results of experimental tests concerning the acquired leaf area and height information of potted plants.

Groups	L_{ta}	L_{ea}	L_{ap} (%)	P_{th} (m)	P_{eh} (m)	P_{hp} (%)
1	29,199	28,417	97.32	0.813	0.795	97.79
2	30,475	30,070	98.67	1.041	1.003	96.35
3	34,548	33,701	97.83	0.929	0.910	97.95
4	38,215	37,262	97.51	0.784	0.777	99.11
5	42,556	42,031	98.77	0.961	0.944	98.23
6	45,194	44,301	98.02	1.052	1.035	98.38
7	35,477	34,969	98.57	0.840	0.822	97.86
8	22,156	21,985	99.23	0.515	0.496	96.31
9	26,571	26,149	98.41	0.678	0.659	97.20
10	20,498	20,358	99.32	0.616	0.598	97.08

3.3. Evaluation of Spraying Operation Performance of the Robotic Platform

3.3.1. Deployed Model Performance

The models were deployed utilising the NVIDIA Jetson Orin Nano (Santa Clara, CA, USA), the central controller of the robotics platform, as the deployment device. TensorRT-FP16 was employed for data quantisation with the objective of accelerating the model inference process. Ablation experiments were conducted on the embedded devices, and the performance of the different models after deployment is presented in Tables 7 and 8. Table 7 shows that the SN-YOLOX Nano-ECA model proposed in this study had the best classification performance, shortest construction time, and fastest classification speed. In comparison to the original YOLOX Nano, the classification precision, recall, and FPS were enhanced by 4.74% and 4.56%, respectively, while the build time was reduced by 11.40 ms. The results of the ablation experiments conducted after model deployment show that that all modules introduced in this study have a beneficial impact on the effectiveness of real-time identification and classification of potted plants. It is also evident that there is almost no degradation in model performance after deployment, which may be due to the fact that although data quantisation simplifies the model by reducing parameters' accuracy, the model's own generalisation capability ensures the inference accuracy of the model.

Table 7. Results of ablation experiments on the embedded device.

Model	YOLOX Nano	ShuffleNetV2	ECA	P (%)	R (%)	Build Phase Time (ms)	FPS
1	on	\	\	93.12	93.96	31.54	26.1
2	\	on	\	91.53	92.44	22.73	32.2
3	on	on	\	95.23	96.37	24.87	34.9
4	on	on	on	97.86	98.52	20.14	37.6

As illustrated in Table 8, the classical lightweight CNNs demonstrated favorable classification performance following deployment. In contrast, the classical CNNs showed average classification performance, with build phase times significantly longer than other models; additionally, the FPS values of VGG16 and ResNet50 were only 4.3 and 6.7, respectively. The deployed SN-YOLOX Nano-ECA model demonstrated optimal precision (97.86%), recall (98.52%), build phase time (20.14 ms), and FPS (37.6), thereby meeting

the criteria for real-time classification of potted plants under different lighting conditions, angles, and occlusions in a real environment.

Table 8. Performance comparison of different models on the embedded device.

Model	P (%)	R (%)	Build Phase Time (ms)	FPS
MobileNetV3	92.41	92.64	28.38	27.5
GhostNet	93.69	94.08	23.22	31.8
YOLOv5s	95.87	95.33	46.49	21.2
VGG16	85.33	94.25	123.66	4.3
ResNet50	94.50	95.27	103.45	6.7
SN-YOLOX	97.86	98.52	20.14	37.6
Nano-ECA				

Images of various potted plants with varying lighting conditions, shooting angles, and backgrounds were captured in real time. The classification efficacy of the SN-YOLOX Nano-ECA model is illustrated in Figure 19, which shows that the model is capable of accurately classifying potted plants in a real complex environment.



Figure 19. Classification results for different varieties of potted plants.

3.3.2. Positioning and Navigation Performance

The constructed five-beacon localisation navigation system is shown in Figure 20, with a site size of 10×10 m. A full combination of navigation walking tests with different moving distances (0, 200, 400, 600, 800, and 1000 cm) along the x- and y-axis was conducted using one of the fixed beacons as the origin. Each experiment was repeated 10 times.

The average moving distance and angular error are shown in Figure 21. It can be observed that the distance and angular error increase gradually from the lower left to the upper right region of the figures. This indicates that the distance and angular error increase with the distance travelled along either axis. The greatest average distance and angle errors, which were 5.598 cm and 0.2245° , respectively, were observed at the destination coordinates (1000 cm, 1000 cm). However, the corresponding precisions were 99.60% and 99.50%, which are sufficient for accurately locating the target potted plant, meeting the practical application requirements for foliar fertiliser dual-face variable spraying.

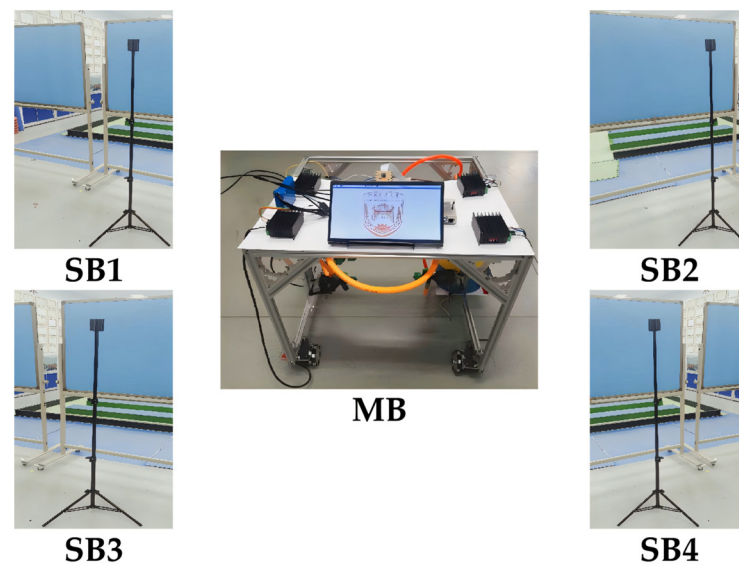


Figure 20. Five-beacon positioning navigation system based on RSSI.

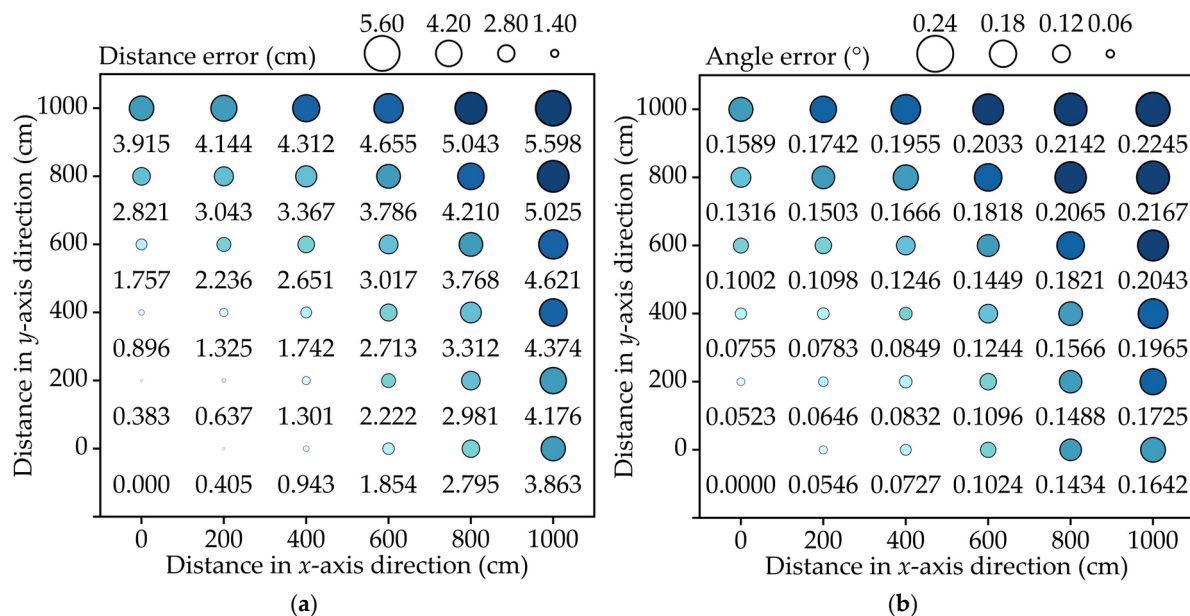


Figure 21. Relationship between navigation travel error and endpoint coordinates. (a) Distance error; (b) Angle error.

3.3.3. Foliar Fertiliser Spraying Performance

The precision of foliar fertiliser dual-face target spraying can be ensured by controlling the nozzle to reach the set height and angle. The nozzle height was set from 40 cm to 80 cm in 4 cm increments based on the main distribution of plant height. Similarly, the nozzle angle was set from 30° to 60° with intervals of 3° based on the main distribution position of the canopy centre. The positioning accuracy test of the height and angle of the novel was carried out. Each group of tests was repeated 10 times, and the average height and angle of the nozzle relative to the ground, along with the standard deviation, were determined. The results are presented in Figure 22a, Figure 22b, Figure 22c, and Figure 22d, respectively. It can be observed that the actual height and angle distribution of the nozzle exhibit a high degree of concentration, with a minimal difference between the set value and the actual measurement. The nozzle action is characterised by high precision, with the relative error in the actual height of the nozzle being less than that of the actual angle. Furthermore, it can be observed that the actual height and angle of the top nozzle are lower than the

set value, while the opposite is true for the bottom nozzle. This can be attributed to the absence of a braking mechanism in the 2D gimbal servo and angle adjust servo, resulting in movement beyond the set value. Nevertheless, the positioning accuracy of the nozzle remains sufficient for the dual-face target precision spraying of foliar fertiliser.

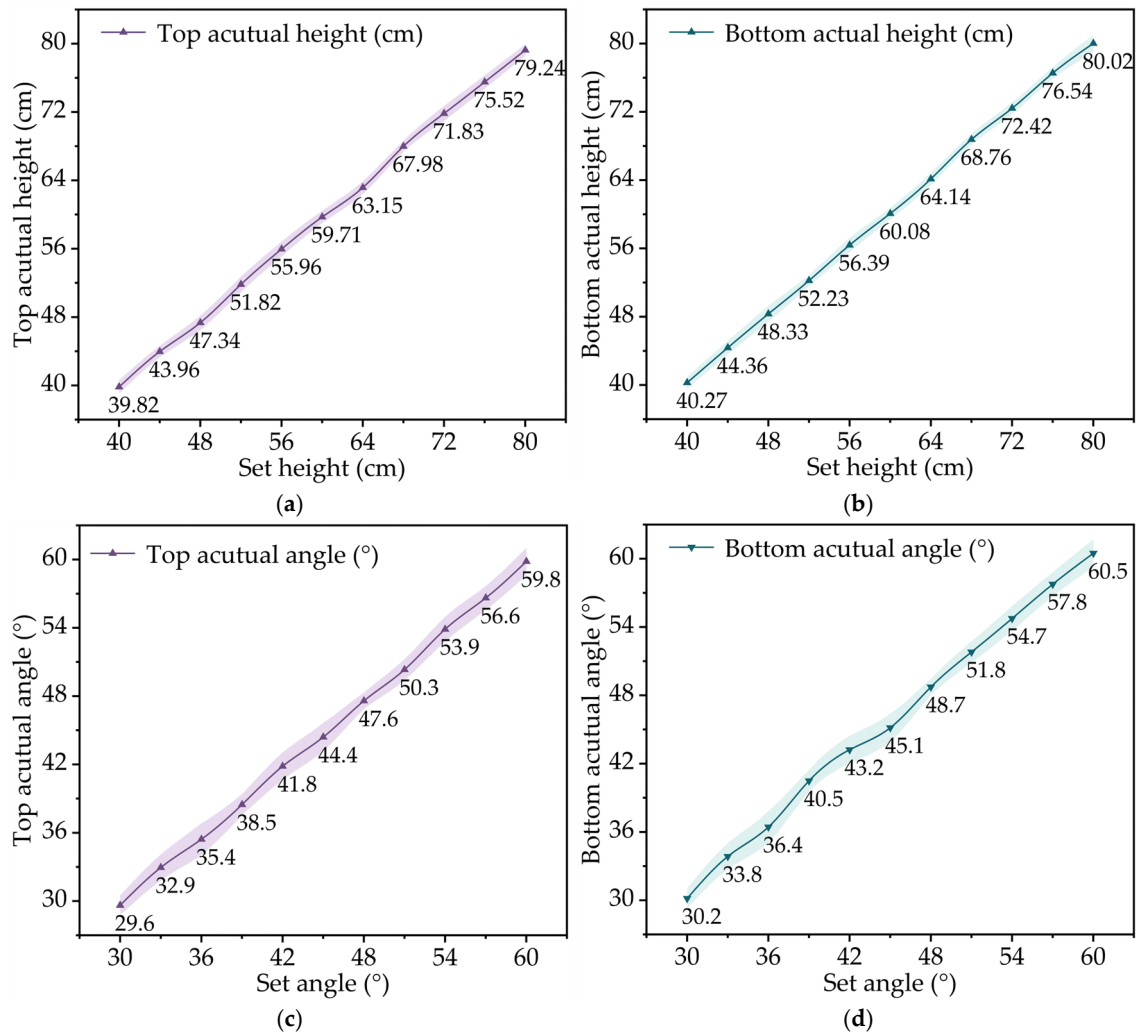


Figure 22. Nozzle positioning accuracy test results. (a,b) are the actual heights of the nozzles on the front and reverse side of the sprayed leaves, respectively. (c,d) are the actual angles of the nozzles on the front and reverse side of the sprayed leaves, respectively.

Ten potted plants were randomly selected for the foliar fertiliser spraying test to evaluate the system's growth state predictions and the accuracy of the spraying amount. The results of the growth state prediction are presented in Table 9. It can be seen that the system accurately predicted the growth status of 10 plants, with the prediction results being consistent with the actual status. This ensures the accuracy of decisions regarding foliar fertiliser spraying. The results of the foliar fertiliser spraying test are presented in Figure 23. It can be observed that the spraying volume of the spray nozzles on the front and the back of the sprayed leaf was nearly identical to the decision-setting value, with only a slight discrepancy. The average accuracy of foliar fertiliser spraying was 97.44%, demonstrating high precision. Overall, the robotic system was able to accurately make decisions on spraying amount and achieve high spraying accuracy, meeting the performance requirements of actual spraying operations.

Table 9. Performance comparison of different models on the embedded device.

Groups	1	2	3	4	5	6	7	8	9	10
Predicted status	Normal	Strong	Normal	Strong	Weak	Strong	Weak	Normal	Normal	Strong
Actual status	Normal	Strong	Normal	Strong	Weak	Strong	Weak	Normal	Normal	Strong

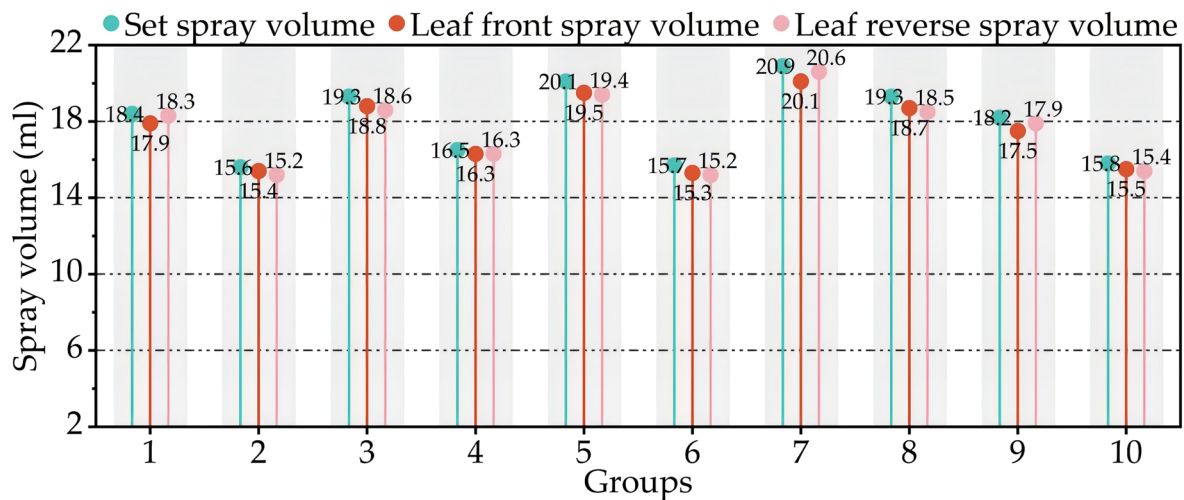


Figure 23. Results of foliar fertiliser spraying test.

4. Discussion

4.1. Analysis of the Practicality of the Model for Identification and Classification of Potted Plants

Deep learning detection models based on computer vision have proven effective in a range of agricultural applications, including crop harvesting [47], weeding [48], disease detection [49], and precision spraying pesticide [50]. However, there is a paucity of research in the field of precision spraying of foliar fertiliser. CNN models are widely used for target classification tasks in agriculture. Recently, Hu et al. proposed the multimodule-YOLOv7-L model [51], which achieved 97.5% real-time classification accuracy for lettuce weed severity, with a classification speed of 37.3 FPS. Shi et al. proposed a lightweight model YOLOv9sPear [52] to improve the accuracy and efficiency of red pear and young pear recognition, achieving a classification accuracy of 0.971, with parameters and FLOPs of 6.23 M and 25.3 G. This paper proposes the SN-YOLOX Nano-ECA model, which is based on the YOLOX Nano model, for the recognition and classification of four common potted plants. The backbone layer is constructed based on ShuffleNetV2, with the ECA attention mechanism introduced in the neck and head. The model's FLOPs and parameters are only 0.16 G and 0.48 M, respectively, rendering it readily deployable on embedded devices. The classification precision for potted plants under different lighting conditions, angles, and occlusions in a real environment reaches 97.86%, with a detection speed of 37.6 FPS, performing at a currently advanced level. This model has the potential to be extended to more types of crop identification and classification. However, only four common ornamental potted plants were selected to construct the dataset in this study, and despite the collection of images under different restrictive conditions to ensure model robustness, the dataset's diversity still needs improvement. Furthermore, the identical number of samples for each category in the dataset resulted in the model training process being unable to attach importance to categories that are challenging to identify. Future research will concentrate on expanding the common potted plant species in the dataset, introducing public image data such as PlantDoc [53] and PlantVillage [54], and collecting images of potted plants in a variety of complex backgrounds representative of real planting environments. Additionally, adjusting the sample distribution ratio is crucial to enhance the model's generalisation ability.

4.2. Analysis of Feasibility of the Dual-Face Target Variable Spraying Methods for the Foliar Fertiliser

Stomata and cuticles are the primary channels for leaf nutrient absorption and are especially concentrated on the reverse of the leaves. Therefore, this study proposes a dual-face target variable spraying method for foliar fertiliser, which assesses the plant growth status based on the leaf area, determines the spatial position based on the plant height, and completes the decision-making on spraying foliar fertiliser in order to achieve dual-face target variable spraying with the nozzle aligned with the canopy centre. The accuracy of the collected leaf area and height information reached 97% and 96%, respectively. However, in addition to leaf area and plant height, phenotypic information such as leaf size, shape, patterning, and colour, etc. can also indicate the plant's growth. Chang et al. developed the Imp-DenseNet model [55], which is capable of accurately classifying wheat leaf rust, stripe rust, and stem rust based on leaf patterning with over 97% accuracy. NDVI is also an important phenotypic information indicator which can reflect crop growth and nutritional status [56]. Ferro et al. used multispectral sensors to obtain NDVI to assess the vigour level in different vineyard areas with the aim of improving orchard management [57]. Hence, further work could introduce additional phenotypic information to optimise decision-making models for foliar fertiliser spraying. Accurate detection of canopy characteristics is essential for precise variable spraying [58], and the canopy volume calculation method in this study poses challenges for irregularly shaped canopies. An RGB-D camera integrates RGB colour images and depth data, enabling the acquisition of the thickness of the target. Qi et al. proposed a method to measure tomato stem thickness using RGB-D data [59], with measurement results in real scenes showing an RMSE of only 1.5 mm between the measurement and the actual diameter. This method has the potential to be employed to improve the calculation accuracy for potted plant canopy volumes in the future. Nevertheless, the foliar fertiliser spraying method proposed in this paper could be extended to other crop production processes that require foliar fertiliser application, with promising prospects for its use.

4.3. Analysis of Reliability of the Spraying Operation of the Robotic Platform

This paper develops a foliar fertiliser dual-face target precision variable spraying robotic platform which can autonomously navigate and walk to the target potted plant to collect images and make foliar fertiliser spraying decisions according to the plant category, leaf area, and height information. Then, the platform controls the pump turn-on time, as well as the height and angle of the nozzles, to complete the foliar fertiliser spraying operation. The positioning and navigation system exhibits a maximum distance and angle error of 5.598 cm and 0.2245°, but there is a risk of cumulative errors. Niu et al. proposed an ECA-ResNet model based on deep learning for mitigating the cumulative ranging error of an indoor UWB positioning system [60], demonstrating a notable reduction in positioning RMSE from 0.7490 m to 0.1731 m. The discrepancies between the actual height and angle of the nozzle and their settings during foliar fertiliser spraying are only 0.328 cm and 0.595°, respectively. Additionally, the error between the spraying amount and the decision-making set value is only 0.46 mL. These values demonstrate the ability to achieve precise variable spraying of foliar fertiliser on the front and reverse side of the target. The inability of the nozzle height and angle adjustment servos to brake independently resulted in action errors. To address this issue, Roshanianfard et al. developed an optimal control methodology for an end-effector servo based on the SOM curve [61], which enabled the precise-alignment picking of pumpkin under the optimal speed and acceleration of the servo. Since the pipeline is pressurised to fill with fertiliser after receiving the control signal, the actual spray amount is slightly lower than the set amount. However, this discrepancy is completely acceptable. In the future, a circulating pipeline with continuous pressure supply can be selected as the supply system for leaf fertiliser. Furthermore, the efficacy of foliar fertiliser spraying will be assessed in the future using indicators such as the droplet

coverage and deposition amount [62,63]. In general, the foliar fertiliser spraying operation robotic platform has excellent performance and reliability.

5. Conclusions

Aiming at the problems of low accuracy, fertiliser utilization, and leaf absorption efficiency, which represent serious wastage of foliar fertiliser, this study proposed an efficient computer vision-based dual-face target precision variable spraying robotic system. The system is capable of autonomously completing a series of tasks, including positioning and navigation, walking, identification and classification of potted plants, spraying decision-making based on phenotypic information, and dual-face target precision variable spraying, thereby achieving excellent performance in foliar fertiliser application. The deployment of the SN-YOLOX Nano-ECA model in this system achieves encouraging real-time potted plant classification performance, with a precision, recall, and FPS of 97.86%, 98.52%, and 37.6. The precision of the leaf area and height information acquired by the system for potted plants exceeded 97% and 96%, respectively, ensuring informed decision-making regarding foliar fertiliser application. During the spraying operation, the accuracy of the moving distance and angle can still reach 99.60% and 99.50%, even at maximum error, ensuring that the real-time image is captured accurately in the optimal position. Meanwhile, the robotic platform maintains alignment of the spray nozzle with the centre of the plant canopy, with an average spraying amount error of only 0.46 mL. The robotic system has the advantages of ease of operation and accurate, efficient spraying, which provides new ideas and references for developing highly efficient and precise variable spraying technology for foliar fertilisers. Furthermore, future research will concentrate on expanding the datasets of potted plant classes and optimising the sample ratio with a view to enhancing the generalisation capacity and applicability. Additionally, the decision-making model for dual-face variable spraying of foliar fertiliser will be further optimised, and the spraying method will be refined.

Author Contributions: Conceptualisation, C.Z. and C.L.; methodology, C.Z.; software, C.Z.; validation, Y.W., S.G. and J.H.; formal analysis, C.Z.; investigation, S.H. and Y.W.; resources, C.L.; data curation, X.J. and J.X.; writing—original draft preparation, C.Z., S.H. and W.W.; writing—review and editing, C.Z. and S.H.; visualisation, C.Z. and S.H.; supervision, C.L.; project administration, C.L.; funding acquisition, C.L. All authors have read and agreed to the published version of the manuscript.

Funding: This research was funded by the Key Laboratory of Modern Agricultural Equipment and Technology (Jiangsu University), Ministry of Education and School of Agricultural Engineering, Jiangsu University (MAET202302); the National Natural Science Foundation of China (52175261).

Data Availability Statement: The data presented in this study are available on request from the corresponding author.

Conflicts of Interest: The authors declare no conflicts of interest.

References

1. Jiang, Y.; Zhang, Y.; Li, H.; Li, H.; Yan, H.; Xing, S. Research on the Control System for the Use of Biogas Slurry as fertiliser. *Agronomy* **2024**, *14*, 1439. [\[CrossRef\]](#)
2. Song, X.; Li, H.; Chen, C.; Xia, H.; Zhang, Z.; Tang, P. Design and Experimental Testing of a Control System for a Solid-fertiliser-Dissolving Device Based on Fuzzy PID. *Agriculture* **2022**, *12*, 1382. [\[CrossRef\]](#)
3. Chauhdary, J.N.; Li, H.; Ragab, R.; Hussain, Z.; Akhlaq, M.; Lakhiar, I.A. Effects of Water Quality and Nitrogen on Wheat Productivity: Experimental and Modelling Study Using the SALTMED Model. *Irrig. Drain.* **2024**, 1–15. [\[CrossRef\]](#)
4. Wang, B.; Wang, Y.; Wang, H.; Mao, H.; Zhou, L. Research on Accurate Perception and Control System of Fertilization Amount for Corn Fertilization Planter. *Front. Plant Sci.* **2022**, *13*, 1074945. [\[CrossRef\]](#) [\[PubMed\]](#)
5. Liu, Y.; Wang, Y.; Ma, G.; Wang, B.; Du, X.; Shi, Q.; Ni, J.; Mao, H. Mechanical Properties of Stem and Physiological-Biochemical Responses of Cucumber under Different N and K Conditions. *Qual. Assur. Saf. Crops Foods* **2022**, *14*, 64–74. [\[CrossRef\]](#)
6. Sanyaolu, M.; Sadowski, A. The Role of Precision Agriculture Technologies in Enhancing Sustainable Agriculture. *Sustainability* **2024**, *16*, 6688. [\[CrossRef\]](#)
7. Martínez García, M.; Ramos Cabral, S.; Pérez Zúñiga, R.; Martínez Rodríguez, L.C.G. Automatic Equipment to Increase Sustainability in Agricultural Fertilization. *Agriculture* **2023**, *13*, 490. [\[CrossRef\]](#)

8. Jia, W.; Wei, Z. Raspberry Pi-Embedded Intelligent Control System for Irrigation and Fertilization Based on Deep Learning. *J. Phys. Conf. Ser.* **2023**, *2504*, 012034. [\[CrossRef\]](#)
9. Loghavi, M.; Behzadi Mackvandi, B. Development of a Target Oriented Weed Control System. *Comput. Electron. Agric.* **2008**, *63*, 112–118. [\[CrossRef\]](#)
10. Bennur, P.J.; Taylor, R.K. Evaluating the Response Time of a Rate Controller Used with a Sensor-Based, Variable Rate Application System. *Appl. Eng. Agric.* **2010**, *26*, 1069–1075. [\[CrossRef\]](#)
11. Lu, Y.; Liu, M.; Li, C.; Liu, X.; Cao, C.; Li, X.; Kan, Z. Precision Fertilization and Irrigation: Progress and Applications. *AgriEngineering* **2022**, *4*, 626–655. [\[CrossRef\]](#)
12. Liu, G.; Hu, H.; Huang, J.; Zhang, J. Lag Time Detection and Position Correction Method of Variable Rate Fertilization. *Trans. Chin. Soc. Agric. Mach.* **2021**, *52*, 74–80. [\[CrossRef\]](#)
13. Zhang, J.; Zhou, Y.; Wu, L.; Xu, L.; Xu, C.; Liang, D.; Ding, Y.; Zhang, Y.; Wang, J.; Li, G. The Yield-Forming Role of Nitrogen in Rice in the Growing Seasons with Variable Thermal Conditions. *Agronomy* **2023**, *13*, 313. [\[CrossRef\]](#)
14. Zhu, Q.; Zhu, Z.; Zhang, H.; Gao, Y.; Chen, L. Design of an Electronically Controlled Fertilization System for an Air-Assisted Side-Deep Fertilization Machine. *Agriculture* **2023**, *13*, 2210. [\[CrossRef\]](#)
15. Zhu, Q.; Zhang, H.; Zhu, Z.; Gao, Y.; Chen, L. Structural Design and Simulation of Pneumatic Conveying Line for a Paddy Side-Deep Fertilisation System. *Agriculture* **2022**, *12*, 867. [\[CrossRef\]](#)
16. Roma, E.; Laudicina, V.A.; Vallone, M.; Catania, P. Application of Precision Agriculture for the Sustainable Management of Fertilization in Olive Groves. *Agronomy* **2023**, *13*, 324. [\[CrossRef\]](#)
17. Tao, Y.; Huang, M.; Zhu, Y.; Tian, T.; Yu, Y.; Wang, H.; Sun, H. Appropriate amount of controlled-release fertilizer for aerial-sown rapeseed at paddy and upland field. *Trans. Chin. Soc. Agric. Eng.* **2024**, *40*, 1–9. [\[CrossRef\]](#)
18. Chen, L.; Xu, Z.; Xie, B.; Liu, L.; Xu, M.; Zheng, Q. Design and Test of Electronic Control System for Unmanned Drive Sprayer. *Trans. Chin. Soc. Agric. Mach.* **2019**, *50*, 122–128. [\[CrossRef\]](#)
19. Diao, Z.; Zhao, M.; Song, Y.; Wu, B.; Wu, Y.; Qian, X.; Wei, Y. Crop line recognition algorithm and realization in precision pesticide system based on machine vision. *Trans. Chin. Soc. Agric. Eng.* **2015**, *31*, 47–52.
20. Zong, Z.; Liu, G.; Zhao, S. Real-Time Localization Approach for Maize Cores at Seedling Stage Based on Machine Vision. *Agronomy* **2020**, *10*, 470. [\[CrossRef\]](#)
21. Gao, J.; Zeng, W.; Ren, Z.; Ao, C.; Lei, G.; Gaiser, T.; Srivastava, A.K. A Fertilization Decision Model for Maize, Rice, and Soybean Based on Machine Learning and Swarm Intelligent Search Algorithms. *Agronomy* **2023**, *13*, 1400. [\[CrossRef\]](#)
22. Wagner, F.; Eltner, A.; Maas, H.-G. River Water Segmentation in Surveillance Camera Images: A Comparative Study of Offline and Online Augmentation Using 32 CNNs. *Int. J. Appl. Earth Obs. Geoinf.* **2023**, *119*, 103305. [\[CrossRef\]](#)
23. Ge, Z.; Liu, S.; Wang, F.; Li, Z.; Sun, J. YOLOX: Exceeding YOLO Series in 2021. *arXiv* **2021**, arXiv:2107.08430. [\[CrossRef\]](#)
24. Redmon, J.; Farhadi, A. YOLOv3: An Incremental Improvement. *arXiv* **2018**, arXiv:1804.02767. [\[CrossRef\]](#)
25. Han, B.; He, L.; Yu, Y.; Lu, W.; Gao, X. General Deformable RoI Pooling and Semi-Decoupled Head for Object Detection. *IEEE Trans. Multimed.* **2024**, *26*, 9410–9422. [\[CrossRef\]](#)
26. Kong, T.; Sun, F.; Liu, H.; Jiang, Y.; Li, L.; Shi, J. FoveaBox: Beyond Anchor-Based Object Detection. *IEEE Trans. Image Process.* **2020**, *29*, 7389–7398. [\[CrossRef\]](#)
27. Wang, C.-Y.; Bochkovskiy, A.; Liao, H.-Y.M. Scaled-YOLOv4: Scaling Cross Stage Partial Network. In Proceedings of the IEEE/CVF Conference on Computer Vision and Pattern Recognition (CVPR), Nashville, TN, USA, 20–25 June 2021; pp. 13024–13033. [\[CrossRef\]](#)
28. Wang, C.-Y.; Mark Liao, H.-Y.; Wu, Y.-H.; Chen, P.-Y.; Hsieh, J.-W.; Yeh, I.-H. CSPNet: A New Backbone That Can Enhance Learning Capability of CNN. In Proceedings of the 2020 IEEE/CVF Conference on Computer Vision and Pattern Recognition Workshops (CVPRW), Seattle, WA, USA, 14–19 June 2020; pp. 1571–1580. [\[CrossRef\]](#)
29. Chollet, F. Xception: Deep Learning with Depthwise Separable Convolutions. In Proceedings of the 2017 IEEE Conference on Computer Vision and Pattern Recognition (CVPR), Honolulu, HI, USA, 21–26 July 2017; pp. 1800–1807. [\[CrossRef\]](#)
30. He, K.; Zhang, X.; Ren, S.; Sun, J. Spatial Pyramid Pooling in Deep Convolutional Networks for Visual Recognition. *IEEE Trans. Pattern Anal. Mach. Intell.* **2015**, *37*, 1904–1916. [\[CrossRef\]](#) [\[PubMed\]](#)
31. Ma, N.; Zhang, X.; Zheng, H.-T.; Sun, J. ShuffleNet V2: Practical Guidelines for Efficient CNN Architecture Design. In Proceedings of the 15th European Conference on Computer Vision (ECCV), Munich, Germany, 8–14 September 2018; pp. 116–131. [\[CrossRef\]](#)
32. Howard, A.; Sandler, M.; Chen, B.; Wang, W.; Chen, L.-C.; Tan, M.; Chu, G.; Vasudevan, V.; Zhu, Y.; Pang, R.; et al. Searching for MobileNetV3. In Proceedings of the 2019 IEEE/CVF International Conference on Computer Vision (ICCV), Seoul, Republic of Korea, 27 October–2 November 2019; pp. 1314–1324. [\[CrossRef\]](#)
33. Han, K.; Wang, Y.; Tian, Q.; Guo, J.; Xu, C.; Xu, C. GhostNet: More Features from Cheap Operations. In Proceedings of the 2020 IEEE/CVF Conference on Computer Vision and Pattern Recognition (CVPR), Seattle, WA, USA, 13–19 June 2020; pp. 1577–1586. [\[CrossRef\]](#)
34. Ren, S.; He, K.; Girshick, R.; Sun, J. Faster R-CNN: Towards Real-Time Object Detection with Region Proposal Networks. *arXiv* **2015**, arXiv:1506.01497. [\[CrossRef\]](#) [\[PubMed\]](#)

35. Hu, J.; Shen, L.; Sun, G. Squeeze-and-Excitation Networks. In Proceedings of the 2018 IEEE/CVF Conference on Computer Vision and Pattern Recognition (CVPR), Salt Lake City, UT, USA, 18–23 June 2018; pp. 7132–7141. [\[CrossRef\]](#)
36. Liu, Y.; Shao, Z.; Hoffmann, N. Global Attention Mechanism: Retain Information to Enhance Channel-Spatial Interactions. *arXiv* **2021**, arXiv:2112.05561. [\[CrossRef\]](#)
37. Wang, Q.; Wu, B.; Zhu, P.; Li, P.; Zuo, W.; Hu, Q. ECA-Net: Efficient Channel Attention for Deep Convolutional Neural Networks. In Proceedings of the 2020 IEEE/CVF Conference on Computer Vision and Pattern Recognition (CVPR), Seattle, WA, USA, 13–19 June 2020; pp. 11534–11542. [\[CrossRef\]](#)
38. Ma, X.; Li, Y.; Wan, L.; Xu, Z.; Song, J.; Huang, J. Classification of Seed Corn Ears Based on Custom Lightweight Convolutional Neural Network and Improved Training Strategies. *Eng. Appl. Artif. Intell.* **2023**, *120*, 105936. [\[CrossRef\]](#)
39. Kumar, A.; Sodhi, S.S. Comparative Analysis of Gaussian Filter, Median Filter and Denoise Autoencoder. In Proceedings of the 2020 7th International Conference on Computing for Sustainable Global Development (INDIACom), New Delhi, India, 12–14 March 2020; pp. 45–51. [\[CrossRef\]](#)
40. Wu, C.; Ma, H.; Jiang, H.; Huang, Z.; Cai, Z.; Zheng, Z.; Wong, C.-H. An Improved Canny Edge Detection Algorithm with Iteration Gradient Filter. In Proceedings of the 2022 6th International Conference on Imaging, Signal Processing and Communications (ICISPC), Kumamoto, Japan, 22–24 July 2022; pp. 16–21. [\[CrossRef\]](#)
41. Payne, W.A.; Wendt, C.W.; Hossner, L.R.; Gates, C.E. Estimating Pearl Millet Leaf Area and Specific Leaf Area. *Agron. J.* **1991**, *83*, 937–941. [\[CrossRef\]](#)
42. Guan, X.; Liu, K.; Qiu, B.; Dong, X.; Xue, X. Extraction of geometric parameters of soybean canopy by airborne 3D laser scanning. *Trans. Chin. Soc. Agric. Eng.* **2017**, *35*, 96–103. [\[CrossRef\]](#)
43. Chen, Y.; Ozkan, H.E.; Zhu, H.; Derksen, R.C.; Krause, C.R. Spray Deposition Inside Tree Canopies from a Newly Developed Variable-Rate Air-Assisted Sprayer. *Trans. ASABE* **2013**, *56*, 1263–1272. [\[CrossRef\]](#)
44. Zafari, F.; Gkelias, A.; Leung, K.K. A Survey of Indoor Localization Systems and Technologies. *IEEE Commun. Surv. Tutor.* **2019**, *21*, 2568–2599. [\[CrossRef\]](#)
45. Simonyan, K.; Zisserman, A. Very Deep Convolutional Networks for Large-Scale Image. *arXiv* **2014**, arXiv:1409.1556. [\[CrossRef\]](#)
46. He, K.; Zhang, X.; Ren, S.; Sun, J. Deep Residual Learning for Image Recognition. In Proceedings of the 2016 IEEE Conference on Computer Vision and Pattern Recognition (CVPR), Las Vegas, NV, USA, 27–30 June 2016; pp. 770–778. [\[CrossRef\]](#)
47. Jing, X.; Jiang, H.; Niu, S.; Zhang, H.; Gilbert Murengami, B.; Wu, Z.; Li, R.; Zhou, C.; Ye, H.; Chen, J.; et al. End-to-End Stereo Matching Network with Two-Stage Partition Filtering for Full-Resolution Depth Estimation and Precise Localization of Kiwifruit for Robotic Harvesting. *Comput. Electron. Agric.* **2024**, *225*, 109333. [\[CrossRef\]](#)
48. Ju, J.; Chen, G.; Lv, Z.; Zhao, M.; Sun, L.; Wang, Z.; Wang, J. Design and Experiment of an Adaptive Cruise Weeding Robot for Paddy Fields Based on Improved YOLOv5. *Comput. Electron. Agric.* **2024**, *219*, 108824. [\[CrossRef\]](#)
49. Liu, W.; Bai, C.; Tang, W.; Xia, Y.; Kang, J. A Lightweight Real-Time Recognition Algorithm for Tomato Leaf Disease Based on Improved YOLOv8. *Agronomy* **2024**, *14*, 2069. [\[CrossRef\]](#)
50. Fan, X.; Chai, X.; Zhou, J.; Sun, T. Deep Learning Based Weed Detection and Target Spraying Robot System at Seedling Stage of Cotton Field. *Comput. Electron. Agric.* **2023**, *214*, 108317. [\[CrossRef\]](#)
51. Hu, R.; Su, W.-H.; Li, J.-L.; Peng, Y. Real-Time Lettuce-Weed Localization and Weed Severity Classification Based on Lightweight YOLO Convolutional Neural Networks for Intelligent Intra-Row Weed Control. *Comput. Electron. Agric.* **2024**, *226*, 109404. [\[CrossRef\]](#)
52. Shi, Y.; Duan, Z.; Qing, S.; Zhao, L.; Wang, F.; Yuwen, X. YOLOv9s-Pear: A Lightweight YOLOv9s-Based Improved Model for Young Red Pear Small-Target Recognition. *Agronomy* **2024**, *14*, 2086. [\[CrossRef\]](#)
53. Singh, D.; Jain, N.; Jain, P.; Kayal, P.; Kumawat, S.; Batra, N. PlantDoc: A Dataset for Visual Plant Disease Detection. *arXiv* **2019**, arXiv:1911.10317. [\[CrossRef\]](#)
54. Khan, A.T.; Jensen, S.M.; Khan, A.R.; Li, S. Plant Disease Detection Model for Edge Computing Devices. *Front. Plant Sci.* **2023**, *14*, 1308528. [\[CrossRef\]](#)
55. Chang, S.; Yang, G.; Cheng, J.; Feng, Z.; Fan, Z.; Ma, X.; Li, Y.; Yang, X.; Zhao, C. Recognition of Wheat Rusts in a Field Environment Based on Improved DenseNet. *Biosyst. Eng.* **2024**, *238*, 10–21. [\[CrossRef\]](#)
56. Zhang, L.; Wang, A.; Zhang, H.; Zhu, Q.; Zhang, H.; Sun, W.; Niu, Y. Estimating Leaf Chlorophyll Content of Winter Wheat from UAV Multispectral Images Using Machine Learning Algorithms under Different Species, Growth Stages, and Nitrogen Stress Conditions. *Agriculture* **2024**, *14*, 1064. [\[CrossRef\]](#)
57. Ferro, M.V.; Catania, P.; Micciché, D.; Pisciotta, A.; Vallone, M.; Orlando, S. Assessment of Vineyard Vigour and Yield Spatio-Temporal Variability Based on UAV High Resolution Multispectral Images. *Biosyst. Eng.* **2023**, *231*, 36–56. [\[CrossRef\]](#)
58. Zhou, H.; Jia, W.; Li, Y.; Ou, M. Method for Estimating Canopy Thickness Using Ultrasonic Sensor Technology. *Agriculture* **2021**, *11*, 1011. [\[CrossRef\]](#)
59. Qi, Z.; Hua, W.; Zhang, Z.; Deng, X.; Yuan, T.; Zhang, W. A Novel Method for Tomato Stem Diameter Measurement Based on Improved YOLOv8-Seg and RGB-D Data. *Comput. Electron. Agric.* **2024**, *226*, 109387. [\[CrossRef\]](#)
60. Niu, Z.; Yang, H.; Zhou, L.; Farag Taha, M.; He, Y.; Qiu, Z. Deep Learning-Based Ranging Error Mitigation Method for UWB Localization System in Greenhouse. *Comput. Electron. Agric.* **2023**, *205*, 107573. [\[CrossRef\]](#)
61. Roshanianfard, A.; Noguchi, N. Pumpkin Harvesting Robotic End-Effector. *Comput. Electron. Agric.* **2020**, *174*, 105503. [\[CrossRef\]](#)

62. Ou, M.; Wang, M.; Zhang, J.; Gu, Y.; Jia, W.; Dai, S. Analysis and Experiment Research on Droplet Coverage and Deposition Measurement with Capacitive Sensor. *Comput. Electron. Agric.* **2024**, *218*, 108743. [[CrossRef](#)]
63. Zhou, H.; Ou, M.; Dong, X.; Zhou, W.; Dai, S.; Jia, W. Spraying Performance and Deposition Characteristics of an Improved Air-Assisted Nozzle with Induction Charging. *Front. Plant Sci.* **2024**, *15*, 1309088. [[CrossRef](#)] [[PubMed](#)]

Disclaimer/Publisher's Note: The statements, opinions and data contained in all publications are solely those of the individual author(s) and contributor(s) and not of MDPI and/or the editor(s). MDPI and/or the editor(s) disclaim responsibility for any injury to people or property resulting from any ideas, methods, instructions or products referred to in the content.